Tau assemblies enter the cytosol of neurons in a cholesterol sensitive manner

Benjamin J. Tuck*[1], Taxiarchis Katsinelos[1], Lauren V. C. Miller[1], Shi Cheng[1], Marina Vaysburd[2], Claire Knox[2], Lucy Tredgett[2], Leo C. James[2], William A. McEwan*[1]

[1] UK Dementia Research Institute at the University of Cambridge, Department of Clinical Neurosciences, Hill Road, Cambridge, CB2 0AH

[2] MRC Laboratory of Molecular Biology, Francis Crick Avenue, Cambridge, CB2 0QH

*Correspondence: bjt44@cam.ac.uk, wm305@cam.ac.uk

Graphical Abstract

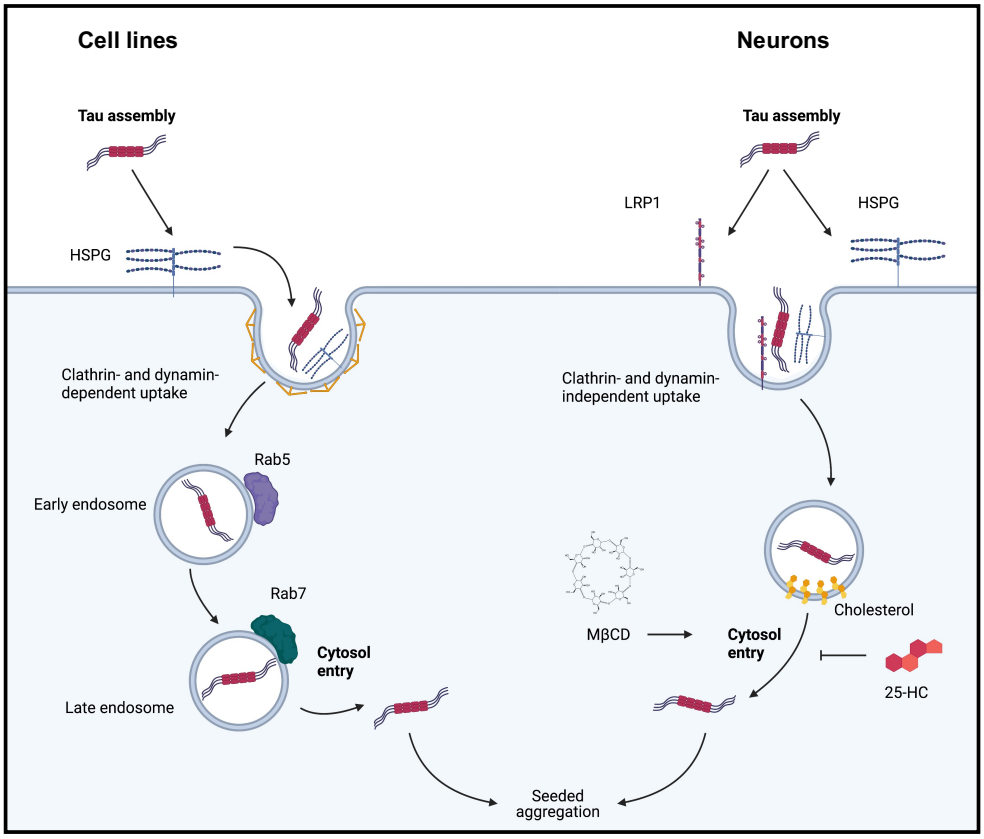

Abstract

The microtubule associated protein tau forms filamentous assemblies in the cytosol of neurons in Alzheimer's disease and other neurodegenerative diseases. Assemblies of tau have been proposed to transit between cells of the brain in a 'prion-like' manner, resulting in templated aggregation of native tau in recipient neurons. Interactions between tau assemblies, surface receptor LRP1 and heparan sulphate proteoglycans promote the uptake of tau assemblies to membrane-bound vesicles. A subsequent escape from these vesicles is postulated for assemblies to enter the cytosol and contact cytosolic tau pools. However, the process by which tau assemblies enter the cytosol is poorly defined. Here we establish assays that permit the study of tau entry in real time and at physiological concentrations. Modulation of entry by genetic or pharmacologic means alters levels of seeded aggregation, confirming the role of cytosolic entry as the rate-limiting, upstream step in seeded aggregation. Entry to HEK293, a commonly used reporter cell line, depended on clathrin-mediated pathways with late endosomal Rab7 GTPase involvement. In contrast, entry to primary neurons was via a clathrin- and dynamin-independent route that was sensitive to cholesterol levels. Extraction of cholesterol from neurons increased tau entry to the cytosol, consistent with cholesterol's established role in maintaining vesicle stability. Importantly, reducing cholesterol levels increased seeded aggregation in both primary neurons and organotypic slice culture models of tau pathology. Finally, we find no evidence that tau assemblies mediate their own entry to the cytosol by membrane rupture. Our results establish cytosolic entry as a distinct event from uptake and is upstream and essential to seeded aggregation. They further describe a cholesterol-sensitive, clathrin-independent pathway of tau entry to the cytosol of neurons.

Introduction

Tauopathies are a group of neurodegenerative diseases characterised by the conversion of microtubule-associated protein tau to highly ordered fibrils (Goedert et al., 2017). Most prominent among these diseases is Alzheimer's disease, which accounts for the majority of the ~50 million dementia cases worldwide. Other tauopathies include fronto-temporal dementia, progressive supranuclear palsy and chronic traumatic encephalopathy. A causal role for tau in neurodegeneration is indicated by more than 50 nonsynonymous and intronic point mutations which lead to dominantly inherited, early onset forms of neurodegenerative disease characterized by the accumulation of tau assemblies in the brain (Goedert, 2018). Two non-mutually exclusive mechanisms are proposed to explain the occurrence of tau fibrils in the diseased brain. First, that nucleation of aggregation occurs within individual cells. Alternatively, that tau assemblies transit between cells, promoting the aggregation of tau in recipient cells in a 'prion-like' manner. This model of aggregation could help explain the observed spatio-temporal spread of tau misfolding in the human brain and is consistent with observations of seeded aggregation in cultured cells (Frost et al., 2009; Kfoury et al., 2012; McEwan et al., 2017; Sanders et al., 2014), and in *in vivo* disease models (Clavaguera et al., 2009, 2013; Guo et al., 2016a; Iba et al., 2013). Nonetheless, the relative contributions of these two mechanisms to human disease progression remains unknown (Mudher et al., 2017). Spread between cells may occur through the uptake of naked tau assemblies, or via extracellular membrane-bound vesicles. Naked tau assemblies are taken up into membrane bound vesicles following interactions between tau and cell-surface heparan sulphate proteoglycans (HSPGs), as well as the recently identified low-density lipoprotein receptor, LRP1 (Holmes et al., 2013; Rauch et al., 2020). Tau is then taken up to membrane-bound compartments via endocytosis and macropinocytosis (Evans et al., 2018; Falcon et al., 2018; Holmes et al., 2013; Wu et al., 2012). For a prion-like mechanism to occur, tau assemblies must subsequently gain access to the cytosol, somehow breeching these intracellular membranes. While the process of tau filament uptake has been comparatively well studied, the transfer of tau from intracellular membrane-bound vesicles to the cytosol remains largely unexplored and remains a critical missing step for assessing the relevance of seeded aggregation to disease progression (De La-Rocque et al., 2021; Mudher et al., 2017).

In this study we develop highly sensitive methods for the detection of tau entry to the cytosol, permitting analysis of entry at physiological concentrations of tau. We find that entry of tau to the cytosol represents the rate-limiting step of seeded aggregation. Accordingly, changing entry levels through pharmacological or genetic means results in a concomitant change in seeded aggregation. Entry occurs in a cell-type dependent manner and the entry pathway of

tau assemblies into human embryonic kidney cells (HEK293) differs substantially from primary neurons. We find that tau does not mediate its own entry to the cytosol of neurons but, rather, enters neurons through a clathrin- and dynamin independent pathway. Entry is sensitive to changes in cellular cholesterol, a lipid which determines membrane physiochemical properties, and a genetic risk factor for neurodegenerative disease (Notkola et al., 1998).

Results

Recombinant Tau-HiBiT assemblies can reconstitute NanoLuc *in vitro*

The study of tau entry to cells has been complicated by the difficulty in reliably distinguishing cytosolic populations from vesicular populations (De La-Rocque et al., 2021). In order to specifically detect the cytosolic fraction of exogenously supplied tau assemblies, we established a live-cell assay relying on split luciferase, NanoLuc (Nluc) (**Fig 1A**). NanoLuc is a 19 kDa luminescent protein engineered from the luciferase of a deep-sea shrimp *Oplophorus gracilirostris.* The enzyme has been split into an 18 kDa subunit (LgBiT) of Nluc and an 11 amino acid peptide (HiBiT) which interact with sub nanomolar affinity. Reconstitution results in the complementation of activity and luminescence in the presence of substrate (Schwinn et al., 2018). We expressed recombinant P301S tau (0N4R isoform) in fusion with a HiBiT tag at the C-terminus in *E. coli* (**Fig. 1B,C**). Assemblies of tau-HiBiT were produced by incubation with heparin and the aggregation kinetics were quantified via thioflavin T fluorescence, a dye which fluoresces strongly when bound to β-sheet amyloid structures. We observed similar aggregation kinetics compared to a tagless variant of tau, suggesting that the HiBiT tag does not interfere with aggregation **(Fig. 1D).** Negative stain electron microscopy revealed filamentous structures with smaller assemblies present after sonication (**Fig. 1E**). To assess the ability of tau-HiBiT assemblies to reconstitute Nluc, we titrated tau-HiBiT assemblies into a fixed concentration of recombinant LgBiT, resulting in a concentration-dependent increase in luminescent signal upon the addition of substrate (**Fig. 1F**). We found the HiBiT tag was as readily accessible in assemblies as it was in monomer, as signal was unchanged between these states (**Fig. S1**). These results confirm that tau-HiBiT can form filaments similar to tagless variants and these assemblies yield a dose-dependent luminescent signal when complexed with LgBiT.

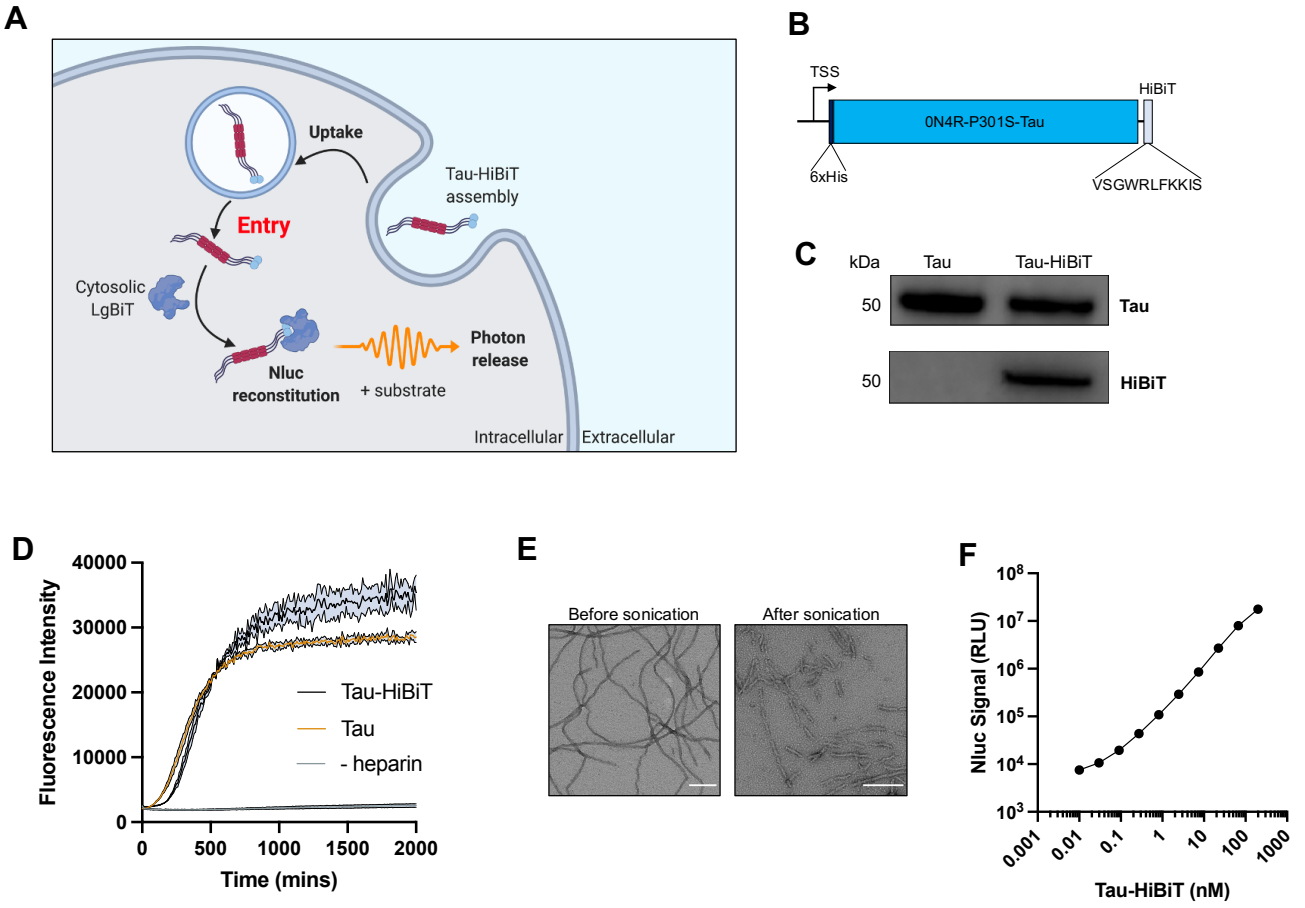

Figure 1: Characterisation of tau-HiBiT assemblies. A) Cartoon depicting the intracellular reconstitution of NanoLuc and the enzymatic production of light through interaction of tau-HiBiT with cytosolic LgBiT. **B)** Depiction of the 6xHis-0N4R-P301S-Tau-HiBiT construct and the amino acid sequence of the HiBiT peptide, to scale relative to tau. **C)** Western blot of 50 ng recombinant tau or tau-HiBiT monomers with anti-tau (DAKO) or anti-HiBiT antibody. **D)** Timecourse of tau-HiBiT and tagless tau (5 μM) aggregation kinetics monitored by thioflavin T (15 μM) fluorescence; n=4. **E)** Representative transmission electron micrographs of heparin-induced tau-HiBiT assemblies before and after a single 15 second sonication cycle. Scale bar, 200 nm. **F)** Representative titration curve of tau-HiBiT assemblies complexed with recombinant LgBiT *in vitro* for 30 minutes; n=4. TSS; transcriptional start site, RLU; relative light units.

Tau-HiBiT assemblies enter cell lines via clathrin-mediated endocytosis

In order to template aggregation, tau assemblies are proposed to cross cell limiting membranes. To measure the entry of tau assemblies to the cell, we expressed LgBiT in the cytosol of human embryonic kidney HEK293 cells, a cell line widely used in the study of seeded tau aggregation (Falcon et al., 2014; Frost et al., 2009; McEwan et al., 2017; Woerman et al., 2016). We expressed LgBiT by lentiviral transduction from the vector pSMPP (Clift et al., 2017) which drives expression from a viral (spleen focus forming virus; SFFV) promoter. We applied sonicated tau-HiBiT assemblies to the cell exterior. This resulted in high luminescence signal that was sensitive to the addition of trypsin, a protease which completely abrogates the luciferase signal of cell free tau-HiBiT:LgBiT complexes (**Fig. S2A,B**). We interpret this as an indication that the bulk of the interaction was extracellular, likely due to leakage or secretion of LgBiT to the media.

We therefore examined if low cytosolic LgBiT concentrations were necessary to establish an assay that reports solely on intracellular tau entry. We reduced cytosolic concentrations of LgBiT first by replacing the SFFV promoter of pSMPP with a mammalian housekeeping promoter (PGK) to generate the vector pPMPP. The cytosolic concentration was further reduced by expressing the protein in fusion with a nuclear localisation signal (nls) and eGFP. The resulting construct (nls-eGFP-LgBiT, abbreviated as NGL) was expressed at ~85:15 nuclear:cytoplasmic ratio and yielded a luciferase signal that was trypsin-insensitive following treatment of cells with tau-HiBiT and addition of a cell-penetrant luciferase substrate (**Fig. 2A-C**). We next titrated tau-HiBiT onto HEK293 cells expressing the construct (HEK-NGL) and observed dose and time-dependent uptake that saturated at around 6 h (**Fig. 2D,E**). These results demonstrate that the assay reports on the real-time entry of tau to live cells with a broad and linear dynamic range.

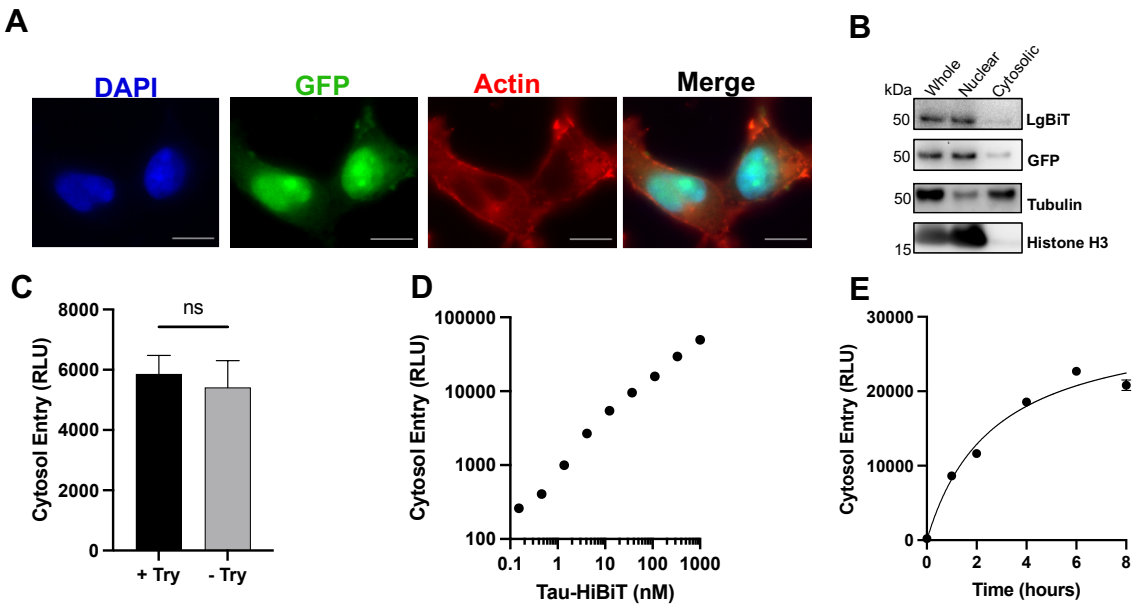

Figure 2: **Tau enters the cytosol of HEK293 cells in a dose-dependent manner**.
A) Immunofluorescence imaging of HEK293 cells expressing nls-eGFP-LgBiT (HEK-NGL), demonstrating nuclear compartmentalisation of NGL. **B)** Western blotting of cytosolic and nuclear fractions of NGL lysates probing for LgBiT, GFP, nuclear marker histone H3 and cytosolic marker, tubulin**. C)** Effect of 10 minutes trypsin protease treatment on luminescent signal in NGL cells prior to substrate addition and signal acquisition; n=≥3. **D)** Representative titration curve of tau-HiBiT assemblies added to HEK-NGL cells for 1 h; n=3. **E)** Representative time-dependency entry curve of 50nM tau-HiBiT assemblies on NGL cells over the course of 8 h; n=3.
NGL; nls-eGFP-LgBiT, nls; nuclear localisation signal, RLU; relative light units, Try; trypsin.

Tau seeding can be dramatically increased by the use of transfection reagents (Holmes et al., 2013), likely owing to enhanced delivery of tau assemblies to the cell interior. To test whether transfection reagents result in increased tau entry to the cytosol, we titrated tau-HiBiT assemblies in the presence and absence of Lipofectamine 2000 (LF) onto HEK-NGL cells. We observed a 50-to-100-fold increase in entry of tau to the cytosol when supplemented with LF (**Fig. 3A**). In HEK293 cells expressing P301S tau-venus (McEwan et al., 2017), we observed an attendant increase in seeded aggregation (**Fig. 3B-D**). These data demonstrate that LF promotes entry to the cell and implicates breeching of intracellular membranes as rate-limiting to seeded aggregation. We next tested whether entry could be inhibited by reducing uptake to the cell. Previous studies have shown that tau uptake occurs via endocytosis in relies on the vesicle coat protein clathrin, as well as the GTPase dynamin (Calafate et al., 2016; Evans et al., 2018, 2020; Shrivastava et al., 2019). We pre-treated cells with the clathrin inhibitor PitStop 2 or the dynamin inhibitor Dyngo 4a. This reduced the uptake of fluorescently labelled transferrin to the cell (**Fig. S2C)** and resulted in a reduction in tau entry to the cytosol **(Fig. 3E).** We also tested the routinely used Na^+/H^+ import channel inhibitor, dimethyl-amiloride (DMA) (Delwig et al., 2006; Grinstein et al., 1989), which inhibits macropinosome

establishment, but observed no change in entry to the HEK-NGL cells (**Fig. 3E**). Incubation of cells at 4ºC, a temperature non-permissive to endocytosis, also prevented tau entry to the cell **(Fig. 3F).** Heparan sulphate proteoglycans (HSPGs) mediate the uptake of tau to intracellular compartments and promote seeded aggregation (Holmes et al., 2013; Rauch et al., 2018). Pre-treatment with surfen hydrate, an agent that binds heparan sulphate, strongly diminished entry in our assay (**Fig. 3F**) as did addition of exogenous heparin to the cell media (**Fig. S2D**). These data together confirm that HSPGs promote entry of tau assemblies to the cytosol of HEK293 cells, and that entry relies upon clathrin and dynamin.

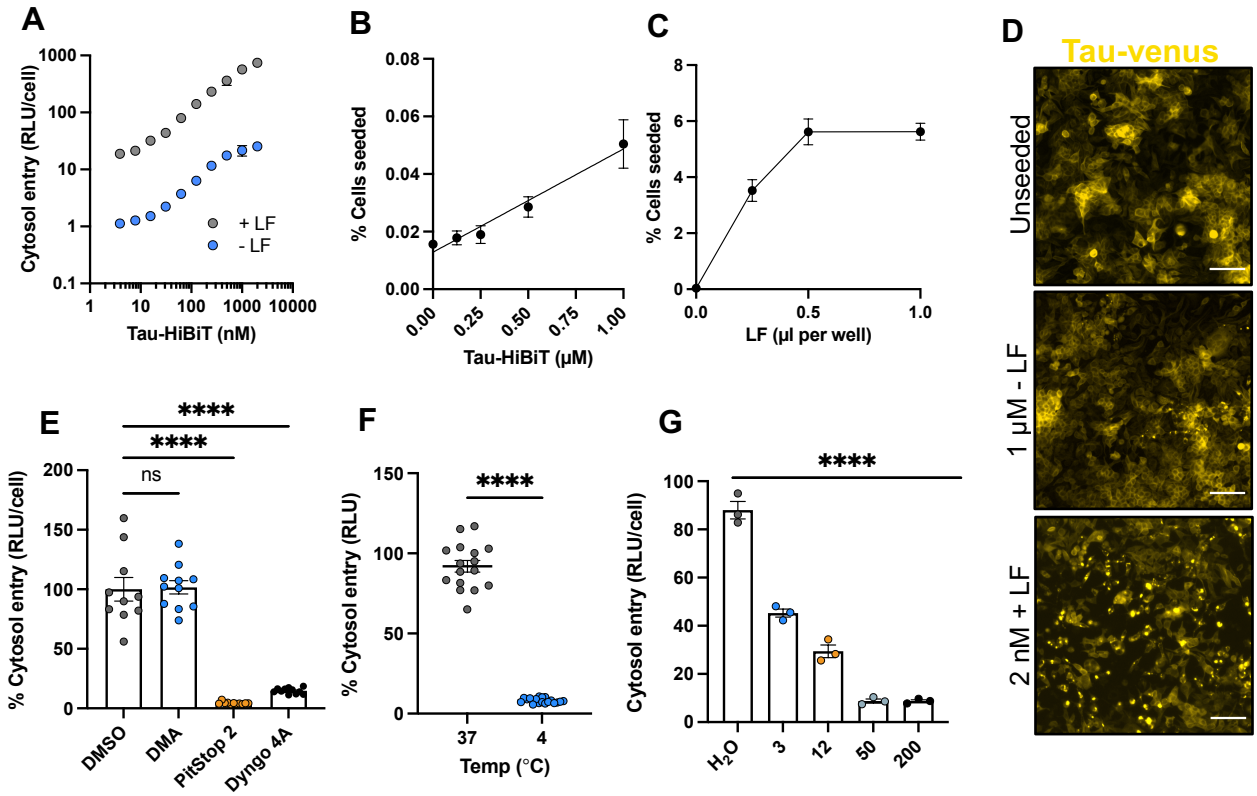

Figure 3: **Tau entry relies on clathrin and dynamin dependent endocytosis**. **A)** Titration of tau-HiBiT in the presence or absence of 1 μl LF after 24 h in NGL cells; n=3. **B)** Representative graph showing the effect of tau-HiBiT assembly concentration on seeded aggregation in HEK293 cells expressing P301S tau-venus; n=3. **C)** Representative graph showing the effect of increasing concentrations of LF on the seeded aggregation of 2 nM tau-HiBiT assemblies; n=3, 5 fields analysed per well. **D)** Fluorescence microscopy images of unseeded control P301S tau-venus cells, cells seeded with 1 μM tau-HiBiT without LF, or cells seeded with 2 nM Tau-HiBiT + 0.5 μl LF. Scale bars, 100 μm. **E)** Effect of uptake inhibitors on tau entry in HEK-NGL cells measured 1 h after addition of 50nM of tau-HiBiT assemblies. HEK-NGL cells were pre-treated with DMA (200 μM), PitStop 2 (10 μM) or Dyngo 4a (20 μM) for 30 minutes before challenge; n=≥3, N=3 independent biological repeats. **F)** Effect of temperature on tau entry. 50nM tau-HiBiT assemblies were supplied to HEK-NGL cells for 1 h at 37°C or 4°C; n=16. **G)** Effect of surfen hydrate on tau entry to HEK-NGL cells at 1 h. Cells were pre-treated for 30 minutes with indicated concentrations of surfen hydrate, or equivalent concentration of solvent (water) before 50nM tau-HiBiT addition; n=3. DMA; dimethyl-amiloride, LF; lipofectamine 2000, RLU; relative light units.

Compromised endolysosomal machinery increases tau entry

After observing the dependency of tau entry on clathrin coat protein and dynamin GTPase, we next investigated the intracellular compartment from which tau assemblies escape. Clathrin- and dynamin-dependent endocytosis results in the enclosure of cargo in a primary endocytic vesicle, which undergoes homotypic fusion to form an early sorting endosome that subsequently traffics throughout the endosomal network with the intraluminal pH simultaneously decreasing (Cullen and Steinberg, 2018). Rab GTPases are crucial effectors of this endosome maturation. To investigate the nature of the compartment from which tau escapes in HEK293 cells, we used siRNA against early endosomal RAB5A or late endosomal RAB7A and performed tau entry assays over the course of 4 h (**Fig 4A,B**). Interestingly, we observed an increase in entry when RAB7A, but not RAB5A, was depleted, suggesting a sensitivity of entry to impaired late endosomal compartments.

Recently, it was shown that compromised function of VPS13D, a ubiquitin binding protein (Anding et al., 2018) promoted the seeded aggregation of tau (Chen et al., 2019). It was proposed that the potential mechanism of augmented tau aggregation may be a result of increased endolysosomal escape of tau seeds. To determine whether VPS13D is involved in maintaining tau assemblies from accessing the cytosol, we depleted VSP13D in HEK-NGL cells and observed a marked increase in tau entry (**Fig 4C,D**). This corroborates the finding that VPS13D is essential to maintaining vesicular integrity and confirms that its depletion promotes entry. We next investigated the role of VPS35, a core constituent of the endosome-to-golgi retromer complex, an essential component of proper endosome sorting. Deficiencies in VPS35 are linked to increased tau burden and late-onset AD (Vagnozzi et al., 2019; Wen et al., 2011) as well as being a known genetic risk in Parkinson's disease (Williams et al., 2017). We treated cells with VPS35 siRNA and, similar to VPS13D depletion, we observed a significant increase in tau entry in knockdown cells but not in control treated cells over 4 h (**Fig 4E,F**). Given that VPS35 interacts with RAB7 (Priya et al., 2015), and that genetic silencing of VPS35 increases tau accumulation (Vagnozzi et al., 2019), our results suggest a mechanism by which mutations associated with the gene may alter the progression of tau pathology. To further support our observations in the entry assay, we depleted VPS35 in HEK293 cells expressing P301S tau-venus and performed seeding assays in the absence of LF. We observed a significant increase in fluorescent puncta corresponding to tau aggregation in VPS35-depleted cells relative to control cells (**Fig 4G,H**). These data demonstrate an essential role for endosome sorting and repair machinery in preventing tau escape to the cytosol.

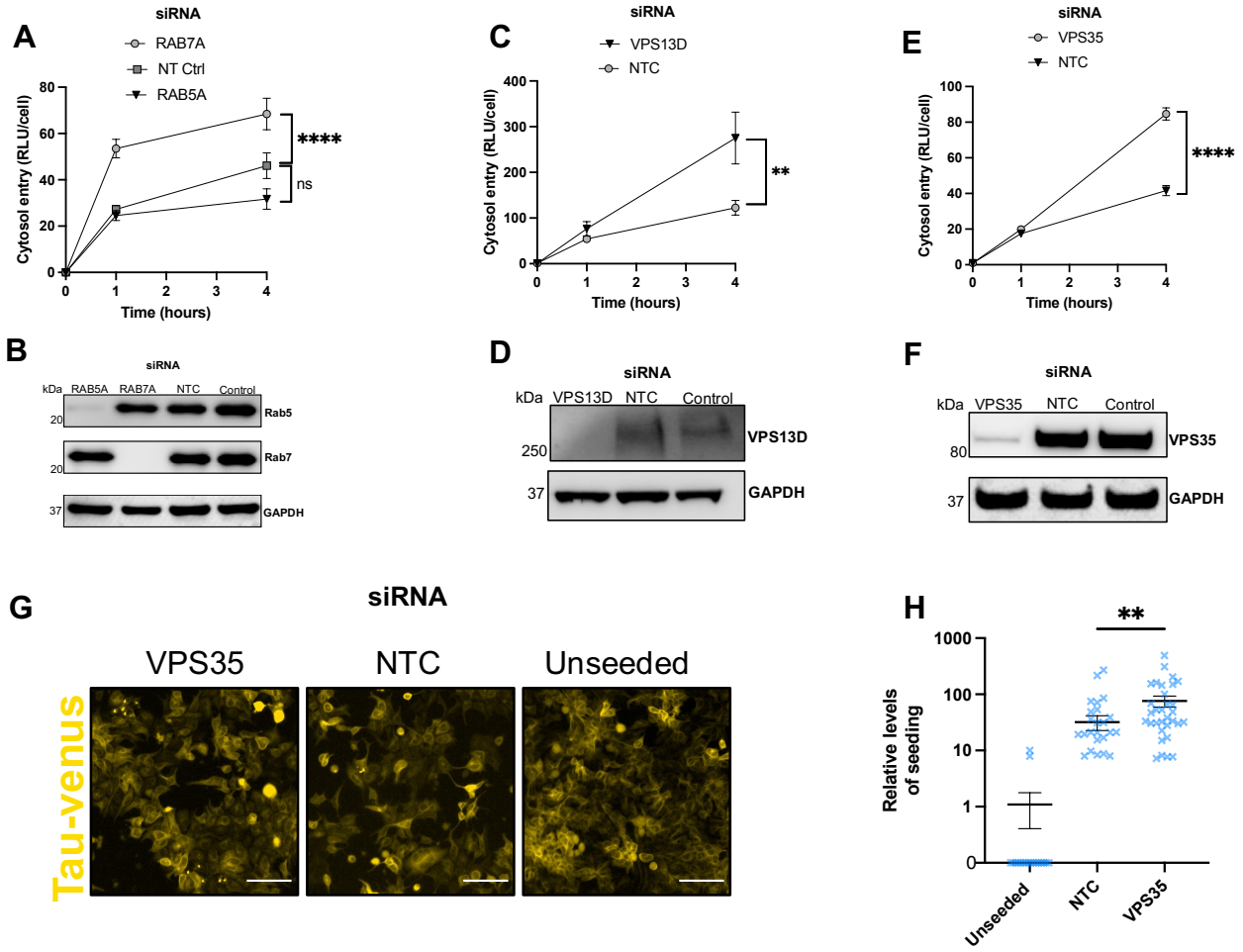

Figure 4: **Endocytic machinery is required to prevent tau access to the cytosol. A)** 4 h timecourse of 50nM tau-HiBiT assemblies following RAB5A or RAB7A knockdown in HEK-NGL cells. Cells were treated with siRNA for 72 h before assaying tau entry; n=3 replicates from N=3 independent experiments. **B)** Western blot of cell lysates in (**A**) for RAB5, RAB7 and GAPDH **C)** 4 h entry time-course of 50nM tau-HiBiT assemblies in HEK-NGL cells following VPS13D knockdown; n=3, N=3 independent biological experiments. **D)** Western blot of cell lysate from (**C**) probing for VPS13D and GAPDH. **E)** 4 h timecourse of 50nM tau-HiBiT assemblies in VPS35 knockdown NGL cells. Cells were treated with siRNA for 72 h before assaying tau entry; n=3, N=2 independent biological replicates with western blot of lysates, **F**). **G)** Representative fluorescence microscopy images of seeded tau-venus cells treated with control or VPS35-targeting siRNA 72 h after the addition of 250 nM exogenous tau-HiBiT assemblies in the absence of lipofectamine. **H)** Quantification of seeded aggregation from tau-venus seeding assays shown in panel **H**; n=6, 5 fields per well analysed. NTC; non-targeting control. RLU; relative light units. Control corresponds to untreated cells.

The mechanism of tau entry is cell-type dependent

To investigate the mechanism of tau entry in a more physiologically relevant system, we adapted our assay to primary neurons derived from wild-type (WT) C57BL/6 mice. We used chimeric particles of adeno-associated virus produced with capsids of types 1 and 2 (AAV1/2) to deliver a self-cleaving variant of the LgBiT reporter from a neuron-specific synapsin (hSyn) promoter. This construct, hSyn::eGFP-P2A-LgBiT-NLS (GPLN), provides eGFP as a fluorescent marker and low levels of nuclear-localised LgBiT (**Fig. 5A-C**). An optimised protocol was established with AAV challenge at 2 days in vitro (DIV) for tau entry assays at 7 DIV, where we see close to 100% of neurons expressing GPLN (**Fig. 5D, Fig. S3A-C)**.

We titrated tau assemblies onto GPLN-neurons and observed a concentration-dependent luciferase signal that was resistant to trypsin, confirming that luminescence originates from an intracellular tau-HiBiT:LgBiT interaction (**Fig 5E, Fig. S3D**). Investigating the entry mechanisms of tau in neurons, we were surprised to find that neither clathrin nor dynamin inhibition with PitStop 2 or Dyngo 4a reduced the entry of tau to the cytosol by any substantial amount (**Fig 5F,G**). Similarly, treatment with DMA to block Na^+/H^+ import channels was unable to prevent entry (**Fig 5H**). We also investigated the requirement for low endosomal pH in entry. We treated neurons acutely with the V-ATPase inhibitor bafilomycin-A at commonly used concentrations to inhibit acidification but avoid downstream effects on autophagy (Yoshimori et al., 1991). We found no requirement for V-ATPase mediated endosomal acidification in tau entry (**Fig. 5I)**. In all cases, neuronal viability was monitored to ensure that experiments reflect entry to healthy cells (**Fig. S3E**). We confirmed that seeded aggregation is similarly insensitive to these inhibitors by challenging neurons with 100 nM tau-HiBiT assemblies in the presence or absence of PitStop 2 or Dyngo 4a. We observed formation of endogenous mouse tau (mTau) aggregates in the presence of inhibitors showed no significant deviation from the solvent treated control neurons **(Fig J,K**). Given that tau can spread in a transsynaptic manner (Calafate et al., 2015; Liu et al., 2012; Wu et al., 2016), we considered whether the observed independence was a result of performing entry assays in cells with improperly formed synapses, which occurs around 7-10 DIV (Grabrucker et al., 2009; Verstraelen et al., 2018). We therefore performed entry assays in 14 DIV neurons but consistently found no role for clathrin or dynamin in entry of tau to the cytosol of neurons **(Fig. S3F).** To further interrogate the entry pathway of tau to neurons, we knocked down mouse Rab5a or Rab7a via siRNA and monitored tau-HiBiT entry over 4 h (**Fig 5L**). Despite a knockdown efficiency of >90% for both proteins and minimal toxicity, we found no role for either protein in tau entry to neurons (**Fig. 5M, Fig. S3G,H**). Our results suggest that tau entry to the cytosol occurs via an alternative mechanism, independent of clathrin-mediated endocytosis. The results in neurons

are in direct contrast to observations in HEK293 cells, suggesting profound differences in the underlying biology between these systems.

Tau assemblies do not mediate their own escape to the cytosol

One possibility is that tau assemblies mediate their own escape from vesicles following uptake by destabilising endosomal membranes. To test this, we titrated tagless tau assemblies in the presence of a constant (50 nM) concentration of tau-HiBiT. If the tagless tau assemblies promote membrane rupturing, we predict this would result in an increase in tau-HiBiT entry. However, in both HEK293 cells and primary neurons, we found no such increase in tau-HiBiT entry, suggesting that tau does not mediate its own entry **(Fig 5N, Fig. S4).** We then used a second membrane integrity assay, wherein a plasmid encoding luciferase is supplied to the extracellular media of HEK293 cells. Addition of membrane rupturing agents results in plasmid transfer to the intracellular environment, promoting luciferase expression. The addition of LF or human adenovirus type 5, which enters cells via endosomal rupture, resulted in 100- to 1,000-fold increases in the levels of luminescence. In contrast, tau assemblies and tau monomer at high concentration (1 μM) resulted in no observable signal above background **(Fig. 5O).**

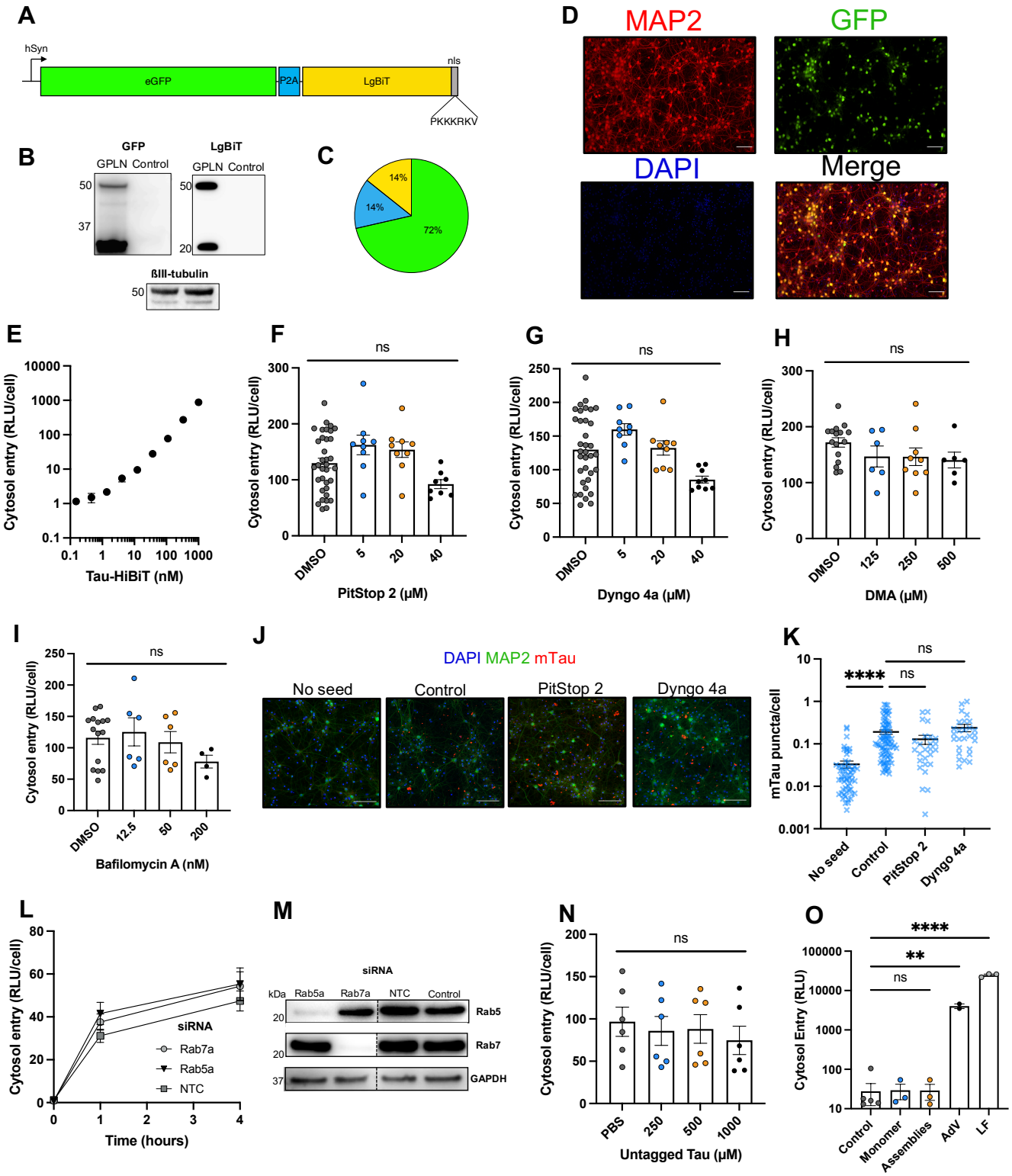

Figure 5: **Tau entry to neurons is clathrin and dynamin independent and is not mediated by tau itself. A)** Cartoon depicting the GPLN construct. **B)** Western blotting 7 DIV WT neurons 5 days post-challenge with AAV1/2-hSyn-GPLN, probing for GFP, LgBiT, and βIII-tubulin as a neuronal loading control. **C)** Pie chart visualising the proportion of protein products translated from the GPLN construct. Green, GFP only; blue, GFP-P2A-LgBiT-nls; yellow, LgBiT-nls only **D)** Fluorescence microscope images of WT 7 DIV primary neurons transduced with AAV1/2-hSyn-GPLN. Scale bars, 100µm. **E)** Representative 1 h entry titration curve of tau-HiBiT assemblies WT 7 DIV primary neurons expressing GPLN; n=3. **F-I)** Effect of clathrin inhibition (PitStop 2), dynamin inhibition (Dyngo 4a) $Na^+\backslash H^+$ import inhibitor DMA or vacuolar ATPase inhibitor bafilomycin A on neuronal tau entry. WT 7 DIV GPLN expressing neurons were pre-treated for 30 minutes with indicated compound and entry of 50nM tau-HiBiT assemblies quantified after a further 1 h. n=≥3 from N=3 independent biological experiments. **J)** Seeded aggregation of tau in DIV 14 WT neurons following pre-treatment for 30 minutes with control solvent (0.1% DMSO), PitStop 2 (10 µM), Dyngo 4a (2 µM) before challenge with 100 nM recombinant tau-HiBiT assemblies at 7 DIV. Drugs were left on cells for the 7-day period. Scale bars, 100 µm. **K)** Quantification of seeded aggregation shown in panel **J.** n=3, 15 fields per well analysed. **L)** 4 h entry timecourse of 50nM tau-HiBiT assemblies in WT 7 DIV neurons expressing GPLN 72 h post-knockdown with 1 µM Rab5a, Rab7a or NTC siRNA; n=3, N=3 independent biological replicates**. M)** Western blotting of neuronal knockdown lysates from panel **L** for Rab5, Rab7, and GAPDH as a loading control. Dashed line represents membrane cropping, full blot available in supplementary. **N)** Effect of untagged tau on cytosolic entry of 50 nM tau-HiBiT assemblies to neurons. Untagged tau aggregates were co-applied to WT neurons expressing GPLN and entry quantified after 1 h; n=3, N=2 independent biological experiments. **O)** Endosomal lysis assay by delivery of nLuc plasmid to HEK293 cells in the presence of excess tau monomer or aggregate (1 µM), adenovirus (MOI 100 IU/cell) or LF (0.2 µl/well)., n=3. AdV, adenovirus type 5; DMA, dimethyl amiloride; GPLN, eGFP-P2A-LgBiT-nls; NTC, non-target control; hSyn, human synapsin promoter; RLU, relative light units.

Lrp1 and HSPGs facilitate the cholesterol-dependent entry of tau to the cytosol of neurons

We next investigated the receptor-dependency of tau entry. We first depleted the low density lipoprotein receptor, Lrp1, recently identified as a receptor for tau uptake (Rauch et al., 2020). Knockdown of this protein substantially decreased tau entry to cells at 4 h after addition (**Fig. 6A,B**). However, entry at 1 h was less affected by Lrp1 depletion, potentially reflecting residual membrane Lrp1 remaining available for uptake followed by receptor internalisation upon tau binding. Addition of heparin to the cell media reduced tau entry in a dose-dependent manner, consistent with a role for cell-surface HSPGs in promoting tau attachment and uptake to neurons (**Fig. 6C).** We next investigated the dependency of cholesterol in neuronal tau entry.

Niemann-Pick disease (NPC) is a genetic disease characterised by the inability to transport cholesterol that displays accumulation of tau filaments (Auer et al., 1995; Garver et al., 2002; Slotte et al., 1989). The apolipoprotein (APOE) gene, which encodes a cholesterol transporting protein, is a genetic risk factor for Alzheimer's disease and primary tauopathy (Rebeck et al., 1993; Zhao et al., 2018). Given these links to cholesterol homeostasis and tau pathology, as well as the contribution of cholesterol to plasma membrane and intracellular vesicle integrity, we hypothesised that cholesterol may modulate tau entry. First, we treated neurons with the cholesterol extracting agent methyl-beta-cyclodextrin (MβCD). Doses in

excess of 5 mM of this compound were found to be cytotoxic to neurons **(S5A).** However, treatment with 2 mM for 2 h before addition of 50 nM tau-HiBiT for 1 h was found to prevent cytotoxic effects of MβCD but yield potent cholesterol extraction, as visualised by staining with the cholesterol-binding dye, filipin (**Fig. 6F, Fig. S5B**). These conditions resulted in a significant increase in tau entry to neurons (**Fig. 6D**). We verified that the effect was due to cholesterol extraction, as treatment with gamma-cyclodextrin (γCD), a cyclodextrin which does not extract cholesterol from membranes, resulted in no significant change in entry compared to the control.

Treatment of cells with the compound 25-hydroxycholesterol (25-HC) results in the accumulation of cholesterol in intracellular membrane-bound organelles (Liu et al., 2018). 25-HC has been shown to inhibit entry of viruses to the cell, including SARS-CoV-2 (Gomes et al., 2018; Zang et al., 2020). We pre-treated neurons for 16 h with 25-HC. Filipin staining revealed accumulation of intracellular cholesterol and we observed a significant reduction in entry (**Fig. 6E,F**). These results suggest that membrane cholesterol is critical to the entry pathway of tau to the cytosol, and may therefore potentially modulate seeded aggregation of tau. To test this, we extracted cellular cholesterol of neurons with a low, tolerated, concentration of MβCD and performed a 7-day seeding assay, where we observed an increase in aggregation of endogenous mouse tau (**Fig. 6G,H)**. These findings demonstrate that tau entry to neurons occurs independently of clathrin-mediated endocytosis but is highly sensitive to membrane cholesterol levels.

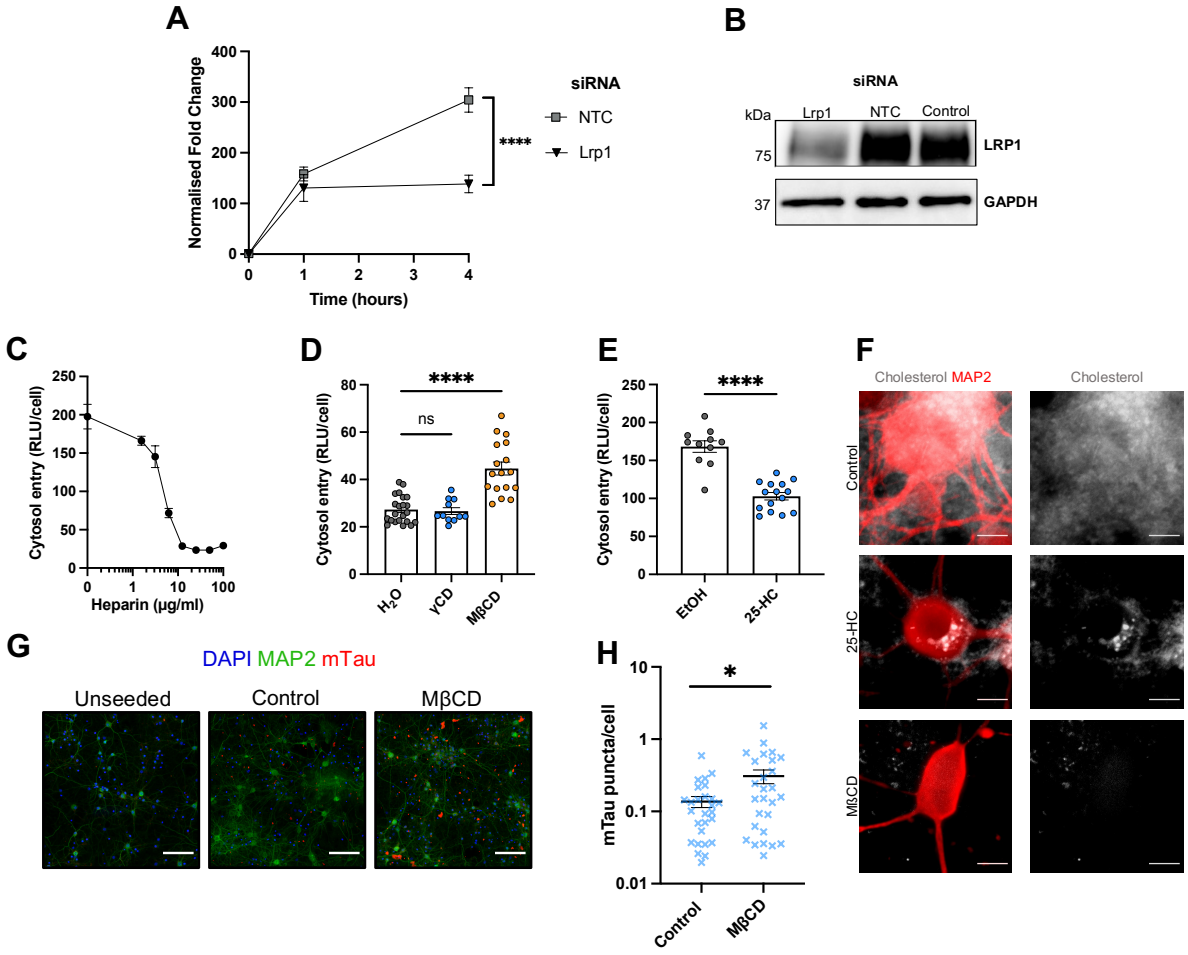

Figure 6: **Tau entry to neurons depends on receptor-mediated uptake and is controlled by cholesterol A)** Time-course of entry of 50 nM tau-HiBiT assemblies in WT DIV 7 neurons expressing GPLN 72 h post-knockdown with of Lrp1 or NTC siRNA; n=3, N=2 independent biological experiments. **B)** Western blotting of neuronal lysates from panel **A** for Lrp1 and Gapdh as a loading control. **C)** Representative entry curve of 50 nM tau-HiBiT assemblies to neurons in the presence of heparin; n=3. **D**) Effect of cholesterol extraction on entry of 50nM tau-HiBiT assemblies in WT DIV 7 neurons expressing GPLN after 1 h. Neurons were pre-treated with γCD (2 mM) or MβCD (2 mM) for 2 h; n=≥4, N=3 independent biological experiments. **E)** Effect of cholesterol transport inhibition on the entry of 50 nM tau-HiBiT assemblies over 1 h in AAV transduced WT 7 DIV neurons. Cells were pre-treated for 16 h with 25-HC (10 µM); n=≥3, N=3 independent biological experiments. **F)** Filipin staining of WT 7 DIV neurons to visualise cellular cholesterol in control (0.1% EtOH), MβCD, (2mM, 2 h) or 25-HC (10 µM, 16 h) cells. Scale bar, 10µm. **G**) Seeded aggregation of tau in DIV 14 WT neurons following pre-treatment with control solvent (0.1% EtOH) or MβCD (200 µM, 2 h) and challenge with 100 nM recombinant tau-HiBiT assemblies at 7 DIV. Drugs were left on cells throughout the 7-day period. Scale bars, 100 µm. **H)** Quantification of seeded aggregation shown in panel **G**. n=3, 15 fields per well analysed. 25-HC; 25-hydroxycholesterol, MβCD; methyl-beta-cyclodextrin, GPLN; eGFP-P2A-LgBiT-nls, NTC; non-targeting control, RLU; relative light units.

Seeded aggregation in organotypic hippocampal slice cultures is sensitive to membrane cholesterol

Our findings have revealed the relationship between tau entry to the cytosol and seeded aggregation in immortalised cells and primary culture models. We next sought to investigate this relationship in organotypic hippocampal slice cultures (OHSCs) which maintain authentic neural architecture and cell-type diversity (Croft et al., 2019). We prepared OHSCs from P301S tau transgenic mice, which develop intracellular tau inclusions by 6 months of age (Allen et al., 2002). OHSCs prepared from these mice do not develop detectable tau pathology unless challenged with tau assemblies (Miller et al., 2021). Tau assemblies were provided to the slices following a 1 day pre-treatment period with MβCD or 25-HC. Tau assemblies were removed after 3 days and the OHSCs were incubated for a further 3 weeks before detection of seeded aggregation using the phospho-tau specific antibody AT8 (**Fig. 7A,B**). Consistent with our observations for tau entry to the cytosol, MβCD increased seeded aggregation by approximately two-fold whereas γCD yielded no statistically significant change (**Fig. 7C**). Treatment with 25-HC resulted in a 30% reduction in seeded aggregation, again consistent with its effect on tau entry (**Fig. 7D**). Together, these results demonstrate an essential role of cellular cholesterol levels in determining the entry of tau assemblies to the cytosol and in determining levels of seeded aggregation.

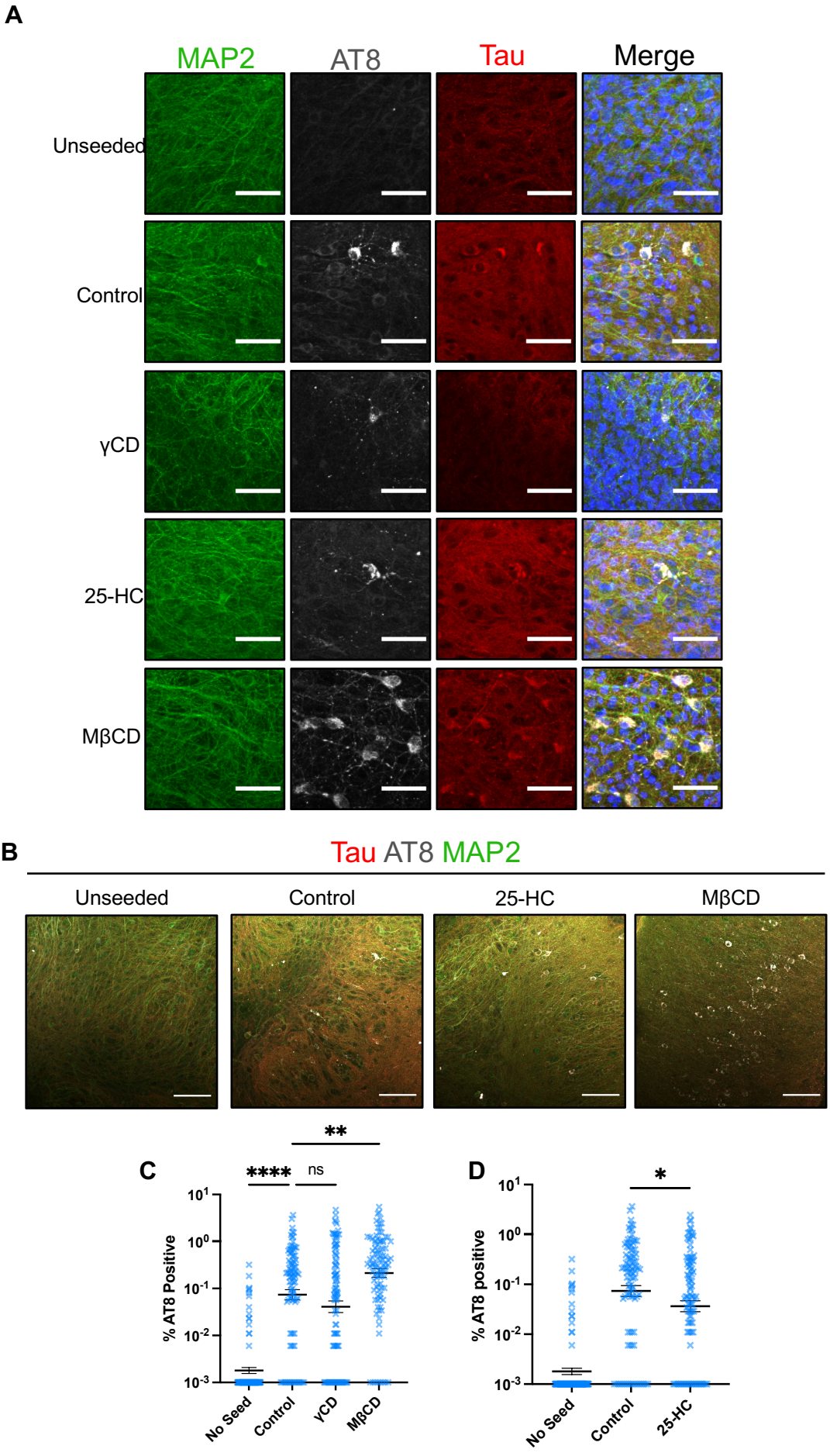

Figure 7: Cholesterol extraction promotes seeded aggregation in organotypic hippocampal slice cultures. A) OHSCs derived from P301S tau transgenic mice were pre-treated with solvent (control, 0.1% EtOH), γCD (200 μM), 25-HC (10 μM) or MβCD (200 μM) for 3 days prior to challenge with 100 nM recombinant tau assemblies for 3 days. Media was exchanged and OHSCs were incubated for 3 weeks before analysis immunofluorescence microscopy. Scale bars, 50 μm, slices from N=6 mice per condition. **B)** Representative images of hippocampal slices visualizing larger areas of the slices, scale bars, 100 μm. **C, D)** Quantification of seeded aggregation in OHSCs treated as in **A** (multiple fields from slices from N=6 mice per condition). * *p*=<0.05 unpaired students t-test. NTC; non-targeting control, γCD; gamma-cyclodextrin, MβCD; methyl-beta-cyclodextrin, 25-HC; 25-hydroxycholesterol, RLU; relative light units.

Discussion

In this study we have developed sensitive assays capable of detecting entry of tau to the cytosol following its application at nanomolar concentrations to the cell exterior. The high sensitivity of the assay means that entry biology can be studied without the use of extra-physiological concentrations of tau, which we have recently found to produce non-linear effects in seeding reactions (Miller et al., 2021). Using these assays, we have described the entry of tau to the cytosol in two cell-based models: HEK293 cells, which are widely used as reporters for seeded aggregation, and neurons, the major site of tau pathology in the brain of AD patients. Entry occurred in a dose-dependent manner over several orders of magnitude, suggesting that extracellular tau concentrations contribute linearly to entry. Levels of entry in HEK293 and neurons were a critical determinant for seeded aggregation, consistent with entry, rather than uptake, being the rate-limiting step to seeded aggregation. We thus quantitatively described a link between entry and seeded aggregation and establish a causal relationship between these processes.

Cytosolic entry of tau is cell-type dependent

We found that tau entry in HEK293 cells is dependent on the coat protein clathrin and the GTPase dynamin, consistent with the frequently described role of canonical endocytosis in human cell tau uptake (De La-Rocque et al., 2021). When we induced endolysosomal dysfunction via genetic knockdown of critical endosomal genes RAB5A and RAB7A, we found only knockdown of RAB7A increased entry. Furthermore, knockdown of VPS35, a core constituent of the retromer complex and a RAB7 effector, similarly increased entry. We therefore consider it likely that tau escapes from late endosomal compartments in HEK293 cells. This dependency was lost, however, in primary mouse neurons. Here, entry of tau occurred through a clathrin- and dynamin-independent pathway with no observable effect of Rab5 or Rab7 depletion. This was not an artefact of using neurons with immature synaptic biology, as 14 DIV cells with highly connected morphology displayed a similar phenotype. Clathrin- and dynamin-independent endocytosis has been described for particular substrates suggesting that tau entry occurs from a specific subset of endosomal compartments (Mayor et al., 2014). Studies that have examined the uptake of tau to neurons demonstrate clathrin-mediated endocytosis (Evans et al., 2018), macropinocytosis (Wu et al., 2013) and a clathrin-independent, dynamin-dependent pathway (Soares et al., 2021). It is therefore possible that several pathways are responsible for tau uptake but tau escape to the cytosol occurs from a subset of compartments. This raises the prospect that molecular dissection of the entry pathway may permit the identification of inhibitors that prevent seeded aggregation by blocking tau entry of tau to the cytosol.

Cholesterol is a critical determinant of tau entry

Cholesterol homeostasis has been repeatedly implicated in the risk and pathogenesis of Alzheimer's disease (van der Kant et al., 2020). Polymorphisms in APOE, the transporter for low density lipoprotein, are the main genetic risk factors for Alzheimer's disease, with the E4 variant increasing the genetic risk in a dose-dependent manner. The involvement of APOE in AD has focussed predominantly on its effects on β-amyloid (Aβ). However, recent data demonstrate that APOE polymorphisms also directly impact tau pathogenesis. APOE polymorphisms affect the risk of progressive supranuclear palsy, which does not feature Aβ pathology (Zhao et al., 2018). Interestingly, homozygosity of the E2 variant, rather than E4, is the genotype associated with highest risk of tauopathy. Consistent with these studies, mouse models have revealed that APOE can modulate tau pathology independent of Aβ (Shi et al., 2019). In the present study, we found that cholesterol levels in neurons are a critical determinant of tau entry. Extraction of cholesterol using MβCD resulted in increased entry, whereas increasing cholesterol accumulation with 25-HC reduced entry. The cholesterol content alters the physiochemical properties of lipid bilayers, by increasing curvature rigidity and reducing the density of lipid packing (Dopico and Tigyi, 2007). Depletion of cholesterol using MβCD alters the mechanical parameters of membranes and renders them susceptible to rupture (Biswas et al., 2019). In contrast, 25-HC treatment increases the availability of cholesterol in phospholipid membranes (Olsen et al., 2011), consistent with the opposing effect we see on tau entry. Together with our findings, these studies suggest that the cholesterol content of tau-bearing compartments is critical to their structural integrity. Loss of integrity, such as following MβCD extraction, results in transfer of tau to the cytosol. The importance of intact cholesterol homeostasis was highlighted by our demonstration that seeded aggregation in neurons and organotypic slice cultures showed concomitant effects in a similar manner as entry when cholesterol content was altered.

Tau escape to the cytosol

It has been suggested that tau escape to the cytosol is dependent on membrane destabilising activities of tau itself. This interpretation is based on the use of cytosolic galectin-3 reporters, which bind to carbohydrates on the luminal leaflet of ruptured vesicles (Calafate et al., 2015; Falcon et al., 2018; Flavin et al., 2017; Polanco and Götz, 2021). The addition of tau assemblies, or cell lysate containing tau assemblies, was found to increase the number of these puncta in those studies. Another study demonstrated that tau assemblies can bind to cell membranes via interactions between the repeat region and phospholipid bilayers, potentially consistent with direct lysis of membranes (Ait-Bouziad et al., 2017). However, in

our study, which directly measures entry to the cytosol, we found no evidence of tau-mediated entry in two separate assays and in both HEK293 and primary neurons. The reasons for these differences are not clear, though may reflect different cell types and fibril preparations, or may reflect inherent differences in directly measuring tau cytosolic entry versus galectin puncta. Our study used recombinant fibrils of a single isotype whereas fibrils prepared from the AD brain comprise all six CNS isoforms. We therefore cannot rule out that other isoforms or tau structures may bear membrane destabilising activity. However, the membrane-interacting domain of tau was mapped to the R2 repeat region (Ait-Bouziad et al., 2017), which is present in the tau isoform used in the present study. Alternatively, membrane destabilisation may be a property of small oligomers, or monomers, rather than the filamentous assemblies used here (Flach et al., 2012; Jones et al., 2012). Our results nonetheless favour an alternative model in which cellular cofactors, rather than tau, are the critical determinants in maintaining the integrity of membrane-bound compartments. Loss of this homeostatic control results in increased entry of tau to the cytosol and a concomitant increase in seeded aggregation. This suggests that cellular/genetic determinants will likely play a pivotal role in this rate-limiting step to tau pathology. The potential dynamic range of this rate-limiting step seeding is demonstrated by lipofectamine, which increased entry and seeded aggregation by >50-fold. In support of this interpretation, Chen et al. also found no evidence of tau mediating its own escape to the cytosol and instead suggested genetic factors influence membrane integrity (Chen et al., 2019). Their results implicated vacuolar sorting proteins as playing a role in maintaining tau out of the cytosol, which we confirm here. Genome-wide association studies and certain dominantly inherited proteopathies implicate several endosome-associated proteins in neurodegeneration (Harold et al., 2009; Lambert et al., 2013; Nixon, 2005). Early endolysosomal genes such as BIN1, PICALM and CD2AP are among the most common genetic polymorphisms associated with late-onset AD, yet there is no consensus on how they influence AD (Acker et al., 2019; Karch and Goate, 2015). Future work should therefore ascertain whether membrane integrity is governed by such genetic risk factors and whether this predisposes to the transit of tau assemblies between cells of the brain.

Summary

Our study provides evidence that tau transit to the neuronal cytosol occurs from an endocytic compartment following uptake by HSPGs and Lrp1. Entry is independent of Rab5/Rab7 GTPases and clathrin in neurons, suggesting that entry occurs from a specific subpopulation of vesicles that lack these cofactors. Maintenance of the unseeded state required cholesterol, an established determinant of membrane stability and susceptibility to rupture. Our study enables the investigation of tau entry as distinct from uptake and will permit investigation of

the genetic and pharmacologic factors that underlie this rate-limiting step in seeded tau aggregation.

Acknowledgements & Funding

We gratefully thank Dr. Filomena Gallo of the Cambridge Advanced Imaging Centre for support & assistance in this work. We thank Annabel Smith and Sophie Sanford of the Cambridge UK DRI for preparation of tau assemblies. We thank Dr Michel Goedert for provision of P301S tau transgenic mice. WAM is a Lister Institute Fellow and supported by a Sir Henry Dale Fellowship jointly funded by the Wellcome Trust and the Royal Society (Grant No. 206248/Z/17/Z). This work was supported by the UK Dementia Research Institute which receives its funding from DRI Ltd, funded by the UK Medical Research Council, Alzheimer's Society and Alzheimer's Research UK. BJT is supported by the Cambridge Trust Vice Chancellor's Award and Hughes Hall Edwin Leong PhD scholarship. This project has received funding from the Innovative Medicines Initiative 2 Joint Undertaking under Grant agreement No. 116060 (IMPRiND). This Joint Undertaking receives support from the European Union's Horizon 2020 research and innovation programme and EFPIA. This work is supported by the Swiss State Secretariat for Education, Research and Innovation (SERI) under contract number 17.00038. Schematic diagrams were prepared in BioRender.

Author contributions

WAM and BJT conceived the study, designed experiments, and wrote the manuscript. BJT performed the majority of experiments with further experiments performed by TK, LCVM and WAM. SC, MJV, CK, LT and LCJ provided reagents and prepared materials essential to the study. All authors edited the manuscript.

Materials and Methods

Antibodies

The following rabbit polyclonal antibodies were acquired from Proteintech; RAB5A (11947-1-AP), RAB7A (55469-1-AP), GFP tag (50430-2-AP), and tubulin (11224-1-AP) as well as secondary goat anti-mouse-HRP (SA00001-1) and goat anti-rabbit-HRP (SA00001-2). LgBiT antibody (N710A) and HiBiT antibody were acquired from Promega. Chicken polyclonal MAP2 (ab5392), rabbit monoclonal histone H3 (ab176842) and rabbit polyclonal VPS13D (ab202285) were purchased from Abcam. Mouse-monoclonal VPS35 (sc-374372) and cyclophilin-B (sc-130626) were purchased from Santa Cruz Biotech. Pan-tau (A0024) DAKO was acquired from Agilent. Anti-mouse tau (T49) was purchased from Sigma (MABN827). anti-phospho tau (AT8) (MN1020), Mouse monoclonal GAPDH loading control (MA5-15738) and Alexa-flour conjugated secondary antibodies were purchased from Thermo Fisher.

Plasmids

The following plasmids were purchased from addgene: pAAV-hSyn-eGFP (#50465), pAdDeltaF6 helper (#112867), pAAV 2/1 (#112862), pAAV 2/2 (#104963). pcRV-Gag-Pol was a gift from Prof Stuart Neil, Kings College London. pMD2G was a gift of Prof Didier Trono, EPFL. HIV-1 expression vector pPMPP was created by replacing the SFFV promoter from pSMPP with a PGK promoter. PGK promoter was amplified using primers WM17-1 TATCGAATTCTTCTACCGGGTAGGGGAGGCG and WM17-2 GACTGGATCCAGGTCGAAAGGCCCGGAGATGA and cloned between EcoRI and BamHI sites of pSMPP. pRK172 was a gift from Dr Michel Goedert, MRC Laboratory of Molecular Biology. NanoLuc-FRB-LgBiT and pNL1.1 were acquired from Promega.

Cell lines

Cells were maintained at 37ºC with 5% CO_2 in a tissue culture incubator. All non-neuronal cells were cultured in complete medium (DMEM supplemented with 10% fetal bovine serum and 1% pen/strep). LgBiT was sub-cloned from the NanoLuc-FRB-LgBiT control vector into the 2nd generation pPMPP-lentiviral vector via PCR. Lentivirus was produced via co-transfection of pPMPP-LgBiT constructs, pcRV-Gagpol and pMD2G vectors into HEK-293T cells with lipofectamine 3000 according to manufacturer instructions (Thermo Fisher, LF300001). Target cells were infected with lentivirus supplemented with 5µg/ml polybrene and subsequently selected with puromycin 48 h post-infection.

Protein Production and Purification

Protein purification was performed as previously described (Katsinelos et al., 2018). Briefly, Human 6xHis-P301S-0N4R-tau-HiBiT was cloned into the bacterial expression vector pRK172 via PCR and expressed in BL21 competent *E. coli* (New England Biolabs, C2530H). Protein expression was induced with 500 µM IPTG overnight at 16ºC. Cells were pelleted and lysed in lysis buffer (1 mM benzamidine, 1 mM PMSF, 1X protease inhibitors, 14 mM β-Mercaptoethanol, 300 mM NaCl, 25 mM HEPES, 30 mM imidazole, 1% NP-40). Lysates were cleared via ultracentrifugation and his-tagged protein purified on the AKTÄ Pure on the HisTrap HP column. Fractions of interest were second round purified via size exclusion chromatography on the Superdex 200 column. Fractions were pooled in PBS with 1mM DTT, concentrated to >3mg/ml and snap frozen in liquid nitrogen followed by long term storage at -80ºC. To aggregate tau, 60µM tau monomer was incubated with 20µM heparin, 2mM DTT and 1x protease inhibitors in PBS for 24-72 h at 37ºC shaking at 250RPM. Tau aggregation was quantified by THT fluorescence readout (excitation 440 nm; emission 510 nm) in the ClarioSTAR plate reader with 5 µM tau aggregates and 15 µM THT.

AAV Production and Titre

eGFP-P2A-LgBiT-nls was cloned into the pAAV-hSyn-eGFP vector genome plasmid via PCR to generate pAAV-hSyn-GPLN. Chimeric particles of adeno-associated virus produced with capsids of types 1 and 2 (AAV1/2) were prepared as previously described (Cheng et al., 2018). Briefly, pAAV-hSyn-GPLN, pAAV2/1, pAAV2/2 and pAdDeltaF6 helper plasmid were co-transfected in HEK293 cells. 48-60 h post-transfection, media and cells were harvested, lysed and viral particles subjected to iodixanol gradient ultracentrifugation. The 40% iodixanol fraction was isolated and concentrated in PBS on Amicon 100 kDa spin columns and frozen at -80°C in single use aliquots. Genome titres were determined via qPCR targeting eGFP (Probe:5'-FAM/CCGACAAGC/ZEN/AGAAGAACGGCATCAA-3') (IDTdna) and purity determined via SDS-PAGE followed by Coomassie staining.

SDS-PAGE and Western Blotting

Samples for western blot were lysed in appropriate volumes of 1 x RIPA buffer (Sigma, R0278) plus 1 x protease inhibitors (Cell signaling technology, 5871S), lysates cleared via centrifugation and resuspended with appropriate volume of 4x NuPAGE LDS sample buffer (Thermo Fisher, NP0007) with 2 mM β-mercaptoethanol and boiled at 100ºC for 10 minutes. Samples were subjected to SDS-PAGE using NuPAGE Bis-Tris 4-12% gels (Thermo Fisher, NP0324BOX) and electroblotted onto a 0.2 µm PVDF membrane using the Bio-Rad Transblot Turbo Transfer System. Transferred membranes were blocked in 5% milk TBS-T (0.1% tween 20 in TBS, blocking buffer) for 1 h at room temperature, and incubated with primary antibody

at desired concentration diluted in blocking buffer at 4ºC overnight. Membranes were repeatedly washed with TBS-T and incubated with secondary HRP- or alexa-flour-conjugated antibody for 1 h at room temperature. Membranes were washed multiple times with TBS-T before being incubated with HRP substrate (Millipore, WBKLS0500) and membranes imaged using a ChemiDoc (Bio-Rad). Subcellular fractionation of the nucleus and cytosol prior to western blotting was performed via the REAP method, as previously described (Suzuki et al., 2010)

Dissections and Primary Neuron Culture

All animal work was licensed under the UK Animals (Scientific Procedures) Act 1986 and approved by the Medical Research Council Animal Welfare and Ethical Review Body. Brains were removed from C57BL/6 mice and primary neurons were isolated as previously described (Beaudoin et al., 2012). The protocol was adapted to produce pooled hippocampal and cortex cultures. Post-dissection, $3x10^4$ cells were seeded per well into a white 96-well poly-L-lysine (RnD Systems, 3438-100-01) coated plate in plating medium (Neurobasal Plus supplemented with 1mM GlutaMAX, 10% Horse Serum, 1% pen/strep and 1x B-27 Plus) for 4 h before a complete media change to maintenance medium (plating medium devoid of serum).

Genetic Knockdown

The following Human onTARGETplus SMARTpool siRNA were purchased from Horizon discovery: non-targeting pool (D-001810-10-05), RAB5A (L-004009-00-0005), RAB7A (L-010388-00-0005), VPS13D (L-021567-02-0005). The following Mouse Accell SMARTpool siRNA were purchased from Horizon discovery: non-targeting pool (D-001910-10-05), Rab5a (E-040855-00-0005), Rab7a (E-040859-01-0005), Lrp1 (E-040764-00-0005), Vps13D (E-050935-00-0005) and Cyclophilin B (D-001920-20-05). Human onTARGETplus siRNA were diluted to 20 µM stock in RNase-free water and cells were transfected with 10 nM siRNA for 3 days with Lipofectamine RNAiMAX transfection reagent (Thermo Fisher, 13778075) in 6 well format. Knockdown cells were re-plated at day 3, and tau-HiBiT entry assayed at day 4. Mouse Accell SMARTpool siRNA were diluted to 100 µM in RNase-free water and added directly to neurons on DIV 3 at a final concentration of 1 µM. Tau entry assay was performed 72 h post-neuronal knockdown

HEK293T Tau Entry Assay

LgBiT expressing HEK293 cells were seeded $2x10^4$ cells per well into white 96-well plates (Greiner bio-one, 655098) coated with poly-L-lysine (Sigma, P4707) in complete DMEM. 12-16 h later, the medium was replaced with 50 µl serum free CO_2 independent medium (Thermo Fisher, 18045088) supplemented with 1 mM sodium pyruvate, 1% pen/strep, 1 mM GlutaMAX

and 50 µl tau-HiBiT solution added to final concentration in 100 µl. Cells were pre-treated for the indicated times with PitStop 2 (Sigma, SML1169), Dyngo 4a (Abcam, ab120689), dimethyl amiloride (Sigma, A125), heparin (Sigma, H3393), surfen hydrate (Sigma, S6951), or supplemented with lipofectamine 2000 (Thermo Fisher, 11668019). After tau incubation, media was aspirated, and cells washed once with PBS. PBS was aspirated and replaced with CO_2 independent medium plus live cell substrate according to manufacturer instructions (Promega Nano-Glo® Live Cell Assay System, N2013). The cells were incubated for 5 minutes and immediately loaded onto the ClarioSTAR plate reader (BMG Labtech) where luminescent signal was quantified at 37ºC. Raw RLU data was normalised to viable cells per well acquired from a PrestoBlue viability assay when expressed as Cytosol entry(RLU/cell).

Neuronal Tau Entry Assay

Primary neurons were infected at DIV 2 with AAV1/2 particles at a multiplicity of 50,000 genome copies per cell to express LgBiT. On day of assay, DIV 7 neurons were 100% media changed to fresh maintenance medium with desired concentration of tau-HiBiT in 100 µl. Neurons were pre-treated by freshly changing to medium supplemented with desired concentration of PitStop 2, Dyngo 4a, dimethyl amiloride, bafilomycin-A (Sigma, SML1661), methyl-β-cyclodextrin (Sigma, C4555), γ-cyclodextrin (Sigma, C4892), 25-hydroxycholesterol (Sigma, H1015) or heparin, followed by addition of tau-HiBiT to final desired concentration. Signal quantification was performed as described for the HEK-293T tau entry assay.

HEK293T seeding assay

The seeding assay was performed as previously described (McEwan et al., 2017). Briefly, 20,000 cells were seeded into poly-L-lysine (Sigma, P4707) coated black 96-well plates in 50 µl OptiMEM (Thermo Fisher, 31985062). Tau assemblies were diluted in OptiMEM and 50 µl added to cells to final concentration in the presence or absence of LF. Cells were incubated at 37ºC and 5% CO_2 for 1 h before the addition of 100 µl complete DMEM to stop the transfection process. Cells were incubated at 37ºC in an IncuCyte S3 Live-Cell Analysis System for 48–72 h after the addition of tau assemblies.

Neuronal seeding assay

Neuronal seeding assays were performed as previously described (Guo et al., 2016b). Briefly, neurons were prepared as described and supplemented with a final concentration of 100 nM tau-HiBiT assemblies at 7 DIV in maintenance medium and incubated at 37ºC and 5% CO_2 until 14 DIV. At 14 DIV, cells were fixed with methanol, nuclei stained with DAPI and epitopes immunofluorescently labelled with anti-MAP2 and anti-mTau (T49) antibodies. Stained

neurons were subjected to high-content imaging of 15 fields per well and tau aggregation quantified. mTau puncta per field were normalised to cell count per field.

OHSC seeding assay

Slices were prepared from P301S tau transgenic pups aged 6-9 days as previously described (Miller et al., 2021). Brains were extracted and maintained in slicing medium (EBSS + 25 mM HEPES) on ice. Brains were bisected along the midline and the medial surface attached to the stage of a Leica VT1200S Vibratome using cyanoacrylate (Loctite Superglue). Sagittal slices of 300 µm thickness were cut and the hippocampus was dissected using sterile needles. Slices were maintained on Millipore membranes (PICM0RG50) with 0.4 µm pore size in 6 well plates with 1 ml Slice Culture Medium (50% MEM with GlutaMAX, 18% EBSS, 6% EBSS + D-glucose, 1% pen/strep, 0.06% nystatin and 25% horse serum). Slices were maintained at 37ºC and 5% CO_2 in a humid atmosphere. Drugs were diluted in 1 ml culture medium and applied to the underside of the slices for 1 day before addition of 100 nM tau. 3 days later, media was removed and fresh medium added without drug or tau. 3 weeks post-challenge, OHSCs were fixed in 4% paraformaldehyde, nuclei stained with DAPI, and MAP2, phopsho-tau (AT8), and tau (DAKO) epitopes immunofluorescently labelled. Stained slice images were acquired using a Zeiss LSM780 confocal microscope with either a 20X or 63X objective lens and images stitched using ZEISS Zen software package.

PrestoBlue Viability Assay

Post-signal acquisition, PrestoBlue™ Cell Viability Reagent (Thermo Fisher, A13261) was added to cells according to manufacturer instructions and incubated for 42 minutes at 37ºC and 5% CO_2. The plate was loaded into the ClarioSTAR plate reader and fluorescence intensity quantified (excitation 540-570 nm; emission 580-610 nm). Total viable cells per well were calculated using a standard curve of known viable cells per well adjusted for background fluorescence.

Plasmid-based endosomal lysis assay

HEK293 cells were plated at $1x10^4$ cells per well in 96 well plates and allowed to adhere overnight. Next day, media was exchanged for serum-free DMEM with pNL1.1 plasmid at 10 ng/µl. Recombinant tau monomers or heparin-assembled tau were added to the media. Lipofectamine 2000 and endosome-destabilising adenovirus type 5 (ViraQuest) were added as positive controls for entry. Plates were examined for NanoLuc luminescence after 24 h.

Transferrin uptake assay

$5x10^5$ HEK293T cells were suspended in serum-free DMEM supplemented with 1% pen/strep and 1 mM GlutaMAX and pre-treated with PitStop 2 (20 μM), Dyngo 4a (20 μM) or DMSO (0.1%) for 30 minutes at 37ºC and 5% CO_2. 50 μg/ml alexa-flour-647-conjugated human transferrin (Thermo Fisher, T23366) was added to the cell suspension and incubated on ice for 5 minutes, followed by 10 minutes at 37ºC and 5% CO_2. Cells were pelleted (500 x g, 5 minutes), acid washed twice (100 mM glycine, 150 mM NaCl in PBS), fixed in 4% PFA (10 mins at room temperature) and subsequently resuspended in FACS buffer (0.5% bovine serum albumin in PBS). Transferrin uptake was then quantified via flow cytometry (CytoFLEX flow cytometer, Beckman Coulter).

Immunofluorescence

Cells were washed once with PBS, fixed with 4% PFA for 15 minutes at room temperature, washed 3 times with PBS followed by permeabilization with 0.1% triton in PBS for 10 minutes at room temperature. Cells were then washed 3 times with PBS, and blocked with 1% BSA in PBS (blocking buffer) for 1 h at room temperature. Primary antibody was diluted to required concentration in blocking buffer and incubated overnight at 4ºC. Antibody was removed, cells were then washed 3 times with PBS and incubated with alexa-flour conjugated secondary antibody in blocking buffer for 1 h at room temp. Secondary antibody was removed, cells washed with PBS 3 times and imaged via fluorescence microscopy. Filipin III staining was performed according to manufacturer instructions (Sigma, SAE0087). For methanol fixation, cells were fixed and permeabilised with ice cold methanol on ice for 3 minutes, followed by 3 half washes with PBS (1X volume added, 0.5X total volume removed) followed by complete aspiration and 3 full washes with PBS. Permeabilised cells were then blocked and stained as described.

Transmission Electron Microscopy

Formation of Tau-HiBiT fibrils was confirmed by uranyl acetate negative stain transmission electron microscopy at the Cambridge Advanced Imaging Centre as previously described (Goedert et al., 1992).

Image analysis

Puncta corresponding to seeded aggregation in HEK-293T and primary neurons were quantified in Fiji using the ComDet plugin (Schindelin et al., 2012). Total puncta per field was normalised to cell count per field via DAPI staining or cell confluency detected by the IncuCyte S3 Live-Cell Analysis software. In neuronal seeding assays, only small puncta colocalised to neurons were quantified. AT8 staining in OHSCs was segmented into a binary threshold and

fields of 150 µM x 150 µM were analysed for % AT8 positive area from slices from N=6 mice per condition.

Statistical Analyses

All statistical analyses were performed via GraphPad Prism software. Differences between multiple means were tested by one-way ANOVA, followed by Tukey's post hoc test unless otherwise indicated in figure 7. Differences between two means were tested by unpaired t-test with Welch's correction. All data represent mean values ± SEM with the following significances: $^{ns}p > 0.05$; $^{*}p \leq 0.05$; $^{**}p \leq 0.01$; $^{***}p \leq 0.001$; and $^{****}p \leq 0.0001$.

References

Acker, Z.P.V., Bretou, M., and Annaert, W. (2019). Endo-lysosomal dysregulations and late-onset Alzheimer's disease: impact of genetic risk factors. Mol Neurodegeneration *14*, 1–20.

Ait-Bouziad, N., Lv, G., Mahul-Mellier, A.-L., Xiao, S., Zorludemir, G., Eliezer, D., Walz, T., and Lashuel, H.A. (2017). Discovery and characterization of stable and toxic Tau/phospholipid oligomeric complexes. Nat Commun *8*, 1678.

Allen, B., Ingram, E., Takao, M., Smith, M.J., Jakes, R., Virdee, K., Yoshida, H., Holzer, M., Craxton, M., Emson, P.C., et al. (2002). Abundant tau filaments and nonapoptotic neurodegeneration in transgenic mice expressing human P301S tau protein. J. Neurosci. *22*, 9340–9351.

Anding, A.L., Wang, C., Chang, T.-K., Sliter, D.A., Powers, C.M., Hofmann, K., Youle, R.J., and Baehrecke, E.H. (2018). Vps13D encodes a ubiquitin binding protein that is required for the regulation of mitochondrial size and clearance. Curr Biol *28*, 287-295.e6.

Auer, I.A., Schmidt, M.L., Lee, V.M., Curry, B., Suzuki, K., Shin, R.W., Pentchev, P.G., Carstea, E.D., and Trojanowski, J.Q. (1995). Paired helical filament tau (PHFtau) in Niemann-Pick type C disease is similar to PHFtau in Alzheimer's disease. Acta Neuropathol *90*, 547–551.

Beaudoin, G.M.J., Lee, S.H., Singh, D., Yuan, Y., Ng, Y.G., Reichardt, L.F., and Arikkath, J. (2012). Culturing pyramidal neurons from the early postnatal mouse hippocampus and cortex. Nature Protocols *7*, 1741–1754.

Biswas, A., Kashyap, P., Datta, S., Sengupta, T., and Sinha, B. (2019). Cholesterol Depletion by MβCD Enhances Cell Membrane Tension and Its Variations-Reducing Integrity. Biophys J *116*, 1456–1468.

Calafate, S., Buist, A., Miskiewicz, K., Vijayan, V., Daneels, G., de Strooper, B., de Wit, J., Verstreken, P., and Moechars, D. (2015). Synaptic Contacts Enhance Cell-to-Cell Tau Pathology Propagation. Cell Rep *11*, 1176–1183.

Calafate, S., Flavin, W., Verstreken, P., and Moechars, D. (2016). Loss of Bin1 Promotes the Propagation of Tau Pathology. Cell Reports *17*, 931–940.

Chen, J.J., Nathaniel, D.L., Raghavan, P., Nelson, M., Tian, R., Tse, E., Hong, J.Y., See, S.K., Mok, S.-A., Hein, M.Y., et al. (2019). Compromised function of the ESCRT pathway promotes endolysosomal escape of tau seeds and propagation of tau aggregation. J Biol Chem *294*, 18952–18966.

Cheng, S., Tereshchenko, J., Zimmer, V., Vachey, G., Pythoud, C., Rey, M., Liefhebber, J., Raina, A., Streit, F., Mazur, A., et al. (2018). Therapeutic efficacy of regulable GDNF expression for Huntington's and Parkinson's disease by a high-induction, background-free "GeneSwitch" vector. Exp Neurol *309*, 79–90.

Clavaguera, F., Bolmont, T., Crowther, R.A., Abramowski, D., Frank, S., Probst, A., Fraser, G., Stalder, A.K., Beibel, M., Staufenbiel, M., et al. (2009). Transmission and spreading of tauopathy in transgenic mouse brain. Nature Cell Biology *11*, 909–913.

Clavaguera, F., Akatsu, H., Fraser, G., Crowther, R.A., Frank, S., Hench, J., Probst, A., Winkler, D.T., Reichwald, J., Staufenbiel, M., et al. (2013). Brain homogenates from human tauopathies induce tau inclusions in mouse brain. Proceedings of the National Academy of Sciences of the United States of America *110*, 9535–9540.

Clift, D., McEwan, W.A., Labzin, L.I., Konieczny, V., Mogessie, B., James, L.C., and Schuh, M. (2017). A Method for the Acute and Rapid Degradation of Endogenous Proteins. Cell *171*, 1692-1706.e18.

Croft, C.L., Futch, H.S., Moore, B.D., and Golde, T.E. (2019). Organotypic brain slice cultures to model neurodegenerative proteinopathies. Molecular Neurodegeneration *14*, 45.

Cullen, P.J., and Steinberg, F. (2018). To degrade or not to degrade: mechanisms and significance of endocytic recycling. Nature Reviews Molecular Cell Biology *19*, 679–696.

De La-Rocque, S., Moretto, E., Butnaru, I., and Schiavo, G. (2021). Knockin' on heaven's door: Molecular mechanisms of neuronal tau uptake. J Neurochem *156*, 563–588.

Delwig, A. von, Hilkens, C.M., Altmann, D.M., Holmdahl, R., Isaacs, J.D., Harding, C.V., Robertson, H., McKie, N., and Robinson, J.H. (2006). Inhibition of macropinocytosis blocks antigen presentation of type II collagen in vitro and in vivo in HLA-DR1 transgenic mice. Arthritis Res Ther *8*, 1–11.

Dopico, A.M., and Tigyi, G.J. (2007). A glance at the structural and functional diversity of membrane lipids. Methods Mol Biol *400*, 1–13.

Evans, L.D., Wassmer, T., Fraser, G., Smith, J., Perkinton, M., Billinton, A., and Livesey Correspondence, F.J. (2018). Extracellular Monomeric and Aggregated Tau Efficiently Enter Human Neurons through Overlapping but Distinct Pathways. Cell Reports *22*, 3612–3624.

Evans, L.D., Strano, A., Campbell, A., Karakoc, E., Iorio, F., Bassett, A.R., and Livesey, F.J. (2020). Whole genome CRISPR screens identify LRRK2-regulated endocytosis as a major mechanism for extracellular tau uptake by human neurons. BioRxiv 2020.08.11.246363.

Falcon, B., Cavallini, A., Angers, R., Glover, S., Murray, T.K., Barnham, L., Jackson, S., O, M.J., Isaacs, A.M., Hutton, M.L., et al. (2014). Conformation Determines the Seeding Potencies of Native and Recombinant Tau Aggregates.

Falcon, B., Noad, J., McMahon, H., Randow, F., and Goedert, M. (2018). Galectin-8-mediated selective autophagy protects against seeded tau aggregation. J Biol Chem *293*, 2438–2451.

Flach, K., Hilbrich, I., Schiffmann, A., Gärtner, U., Krüger, M., Leonhardt, M., Waschipky, H., Wick, L., Arendt, T., and Holzer, M. (2012). Tau oligomers impair artificial membrane integrity and cellular viability. J Biol Chem *287*, 43223–43233.

Flavin, W.P., Bousset, L., Green, Z.C., Chu, Y., Skarpathiotis, S., Chaney, M.J., Kordower, J.H., Melki, R., and Campbell, E.M. (2017). Endocytic vesicle rupture is a conserved mechanism of cellular invasion by amyloid proteins. Acta Neuropathol. *134*, 629–653.

Frost, B., Jacks, R.L., and Diamond, M.I. (2009). Propagation of Tau Misfolding from the Outside to the Inside of a Cell. Journal of Biological Chemistry *284*, 12845–12852.

Garver, W.S., Krishnan, K., Gallagos, J.R., Michikawa, M., Francis, G.A., and Heidenreich, R.A. (2002). Niemann-Pick C1 protein regulates cholesterol transport to the trans-Golgi network and plasma membrane caveolae. J Lipid Res *43*, 579–589.

Goedert, M. (2018). Tau filaments in neurodegenerative diseases. FEBS Lett *592*, 2383–2391.

Goedert, M., Spillantini, M.G., Cairns, N.J., and Crowther, R.A. (1992). Tau proteins of alzheimer paired helical filaments: Abnormal phosphorylation of all six brain isoforms. Neuron *8*, 159–168.

Goedert, M., Eisenberg, D.S., and Crowther, R.A. (2017). Propagation of Tau Aggregates and Neurodegeneration. Annu. Rev. Neurosci. *40*, 189–210.

Gomes, B., Gonçalves, S., Disalvo, A., Hollmann, A., and Santos, N.C. (2018). Effect of 25-hydroxycholesterol in viral membrane fusion: Insights on HIV inhibition. Biochimica et Biophysica Acta (BBA) - Biomembranes *1860*, 1171–1178.

Grabrucker, A., Vaida, B., Bockmann, J., and Boeckers, T.M. (2009). Synaptogenesis of hippocampal neurons in primary cell culture. Cell Tissue Res *338*, 333.

Grinstein, S., Rotin, D., and Mason, M.J. (1989). Na+/H+ exchange and growth factor-induced cytosolic pH changes. Role in cellular proliferation. Biochim Biophys Acta *988*, 73–97.

Guo, J.L., Narasimhan, S., Changolkar, L., He, Z., Stieber, A., Zhang, B., Gathagan, R.J., Iba, M., McBride, J.D., Trojanowski, J.Q., et al. (2016a). Unique pathological tau conformers from Alzheimer's brains transmit tau pathology in nontransgenic mice. The Journal of Experimental Medicine *213*, 2635–2654.

Guo, J.L., Narasimhan, S., Changolkar, L., He, Z., Stieber, A., Zhang, B., Gathagan, R.J., Iba, M., McBride, J.D., Trojanowski, J.Q., et al. (2016b). Unique pathological tau conformers from Alzheimer's brains transmit tau pathology in nontransgenic mice. J. Exp. Med. *213*, 2635–2654.

Harold, D., Abraham, R., Hollingworth, P., Sims, R., Gerrish, A., Hamshere, M.L., Pahwa, J.S., Moskvina, V., Dowzell, K., Williams, A., et al. (2009). Genome-wide association study identifies variants at *CLU* and *PICALM* associated with Alzheimer's disease. Nature Genetics *41*, 1088–1093.

Holmes, B.B., DeVos, S.L., Kfoury, N., Li, M., Jacks, R., Yanamandra, K., Ouidja, M.O., Brodsky, F.M., Marasa, J., Bagchi, D.P., et al. (2013). Heparan sulfate proteoglycans mediate internalization and propagation of specific proteopathic seeds. Proceedings of the National Academy of Sciences *110*, E3138–E3147.

Iba, M., Guo, J.L., McBride, J.D., Zhang, B., Trojanowski, J.Q., and Lee, V.M.-Y. (2013). Synthetic tau fibrils mediate transmission of neurofibrillary tangles in a transgenic mouse model of Alzheimer's-like tauopathy. The Journal of Neuroscience : The Official Journal of the Society for Neuroscience *33*, 1024–1037.

Jones, E.M., Dubey, M., Camp, P.J., Vernon, B.C., Biernat, J., Mandelkow, E., Majewski, J., and Chi, E.Y. (2012). Interaction of tau protein with model lipid membranes induces tau structural compaction and membrane disruption. Biochemistry *51*, 2539–2550.

van der Kant, R., Goldstein, L.S.B., and Ossenkoppele, R. (2020). Amyloid-β-independent regulators of tau pathology in Alzheimer disease. Nat Rev Neurosci *21*, 21–35.

Karch, C.M., and Goate, A.M. (2015). Alzheimer's disease risk genes and mechanisms of disease pathogenesis. Biol Psychiatry *77*, 43–51.

Katsinelos, T., Zeitler, M., Dimou, E., Ruiz De Almodovar, C., Nickel, W., Correspondence, T.R.J., Karakatsani, A., M€, H.-M., Nachman, E., Steringer, J.P., et al. (2018). Unconventional Secretion Mediates the Trans-cellular Spreading of Tau Article Unconventional Secretion Mediates the Trans-cellular Spreading of Tau. Cell Reports.

Kfoury, N., Holmes, B.B., Jiang, H., Holtzman, D.M., and Diamond, M.I. (2012). Trans-cellular propagation of Tau aggregation by fibrillar species. Journal of Biological Chemistry.

Lambert, J.-C., Ibrahim-Verbaas, C.A., Harold, D., Naj, A.C., Sims, R., Bellenguez, C., Jun, G., DeStefano, A.L., Bis, J.C., Beecham, G.W., et al. (2013). Meta-analysis of 74,046 individuals identifies 11 new susceptibility loci for Alzheimer's disease. Nature Genetics *45*, 1452–1458.

Liu, L., Drouet, V., Wu, J.W., Witter, M.P., Small, S.A., Clelland, C., and Duff, K. (2012). Trans-synaptic spread of tau pathology in vivo. PLoS ONE *7*, e31302.

Liu, Y., Wei, Z., Ma, X., Yang, X., Chen, Y., Sun, L., Ma, C., Miao, Q.R., Hajjar, D.P., Han, J., et al. (2018). 25-Hydroxycholesterol activates the expression of cholesterol 25-hydroxylase in an LXR-dependent mechanism[S]. Journal of Lipid Research *59*, 439–451.

Mayor, S., Parton, R.G., and Donaldson, J.G. (2014). Clathrin-independent pathways of endocytosis. Cold Spring Harb Perspect Biol *6*.

McEwan, W.A., Falcon, B., Vaysburd, M., Clift, D., Oblak, A.L., Ghetti, B., Goedert, M., and James, L.C. (2017). Cytosolic Fc receptor TRIM21 inhibits seeded tau aggregation. Proceedings of the National Academy of Sciences *114*, 574–579.

Miller, L.V.C., Mukadam, A.S., Durrant, C.S., Vaysburd, M.J., Katsinelos, T., Tuck, B.J., Sanford, S., Sheppard, O., Knox, C., Cheng, S., et al. (2021). Tau assemblies do not behave like independently acting prion-like particles in mouse neural tissue. Acta Neuropathol Commun *9*, 41.

Mudher, A., Colin, M., Dujardin, S., Medina, M., Dewachter, I., Alavi Naini, S.M., Mandelkow, E.-M., Mandelkow, E., Buée, L., Goedert, M., et al. (2017). What is the evidence that tau pathology spreads through prion-like propagation? Acta Neuropathol Commun *5*, 99.

Nixon, R.A. (2005). Endosome function and dysfunction in Alzheimer's disease and other neurodegenerative diseases. Neurobiol. Aging *26*, 373–382.

Notkola, I.L., Sulkava, R., Pekkanen, J., Erkinjuntti, T., Ehnholm, C., Kivinen, P., Tuomilehto, J., and Nissinen, A. (1998). Serum total cholesterol, apolipoprotein E epsilon 4 allele, and Alzheimer's disease. Neuroepidemiology *17*, 14–20.

Olsen, B.N., Schlesinger, P.H., Ory, D.S., and Baker, N.A. (2011). 25-Hydroxycholesterol Increases the Availability of Cholesterol in Phospholipid Membranes. Biophysical Journal *100*, 948–956.

Polanco, J.C., and Götz, J. (2021). Exosomal and vesicle-free tau seeds - propagation and convergence in endolysosomal permeabilization. FEBS J.

Priya, A., Kalaidzidis, I.V., Kalaidzidis, Y., Lambright, D., and Datta, S. (2015). Molecular insights into Rab7-mediated endosomal recruitment of core retromer: deciphering the role of Vps26 and Vps35. Traffic *16*, 68–84.

Rauch, J.N., Chen, J.J., Sorum, A.W., Miller, G.M., Sharf, T., See, S.K., Hsieh-Wilson, L.C., Kampmann, M., and Kosik, K.S. (2018). Tau Internalization is Regulated by 6-O Sulfation on Heparan Sulfate Proteoglycans (HSPGs). Scientific Reports *8*, 6382.

Rauch, J.N., Luna, G., Guzman, E., Audouard, M., Challis, C., Sibih, Y.E., Leshuk, C., Hernandez, I., Wegmann, S., Hyman, B.T., et al. (2020). LRP1 is a master regulator of tau uptake and spread. Nature.

Rebeck, G.W., Reiter, J.S., Strickland, D.K., and Hyman, B.T. (1993). Apolipoprotein E in sporadic Alzheimer's disease: allelic variation and receptor interactions. Neuron *11*, 575–580.

Sanders, D.W., Kaufman, S.K., DeVos, S.L., Sharma, A.M., Mirbaha, H., Li, A., Barker, S.J., Foley, A.C., Thorpe, J.R., Serpell, L.C., et al. (2014). Distinct Tau Prion Strains Propagate in Cells and Mice and Define Different Tauopathies. Neuron *82*, 1271–1288.

Schindelin, J., Arganda-Carreras, I., Frise, E., Kaynig, V., Longair, M., Pietzsch, T., Preibisch, S., Rueden, C., Saalfeld, S., Schmid, B., et al. (2012). Fiji: an open-source platform for biological-image analysis. Nat Methods *9*, 676–682.

Schwinn, M.K., Machleidt, T., Zimmerman, K., Eggers, C.T., Dixon, A.S., Hurst, R., Hall, M.P., Encell, L.P., Binkowski, B.F., and Wood, K.V. (2018). CRISPR-Mediated Tagging of Endogenous Proteins with a Luminescent Peptide. ACS Chem Biol *13*, 467–474.

Shi, Y., Manis, M., Long, J., Wang, K., Sullivan, P.M., Remolina Serrano, J., Hoyle, R., and Holtzman, D.M. (2019). Microglia drive APOE-dependent neurodegeneration in a tauopathy mouse model. J Exp Med *216*, 2546–2561.

Shrivastava, A.N., Redeker, V., Pieri, L., Bousset, L., Renner, M., Madiona, K., Mailhes-Hamon, C., Coens, A., Buée, L., Hantraye, P., et al. (2019). Clustering of Tau fibrils impairs

the synaptic composition of α3-Na+/K+-ATPase and AMPA receptors. The EMBO Journal *38*, e99871.

Slotte, J.P., Hedström, G., and Bierman, E.L. (1989). Intracellular transport of cholesterol in type C Niemann-Pick fibroblasts. Biochim Biophys Acta *1005*, 303–309.

Soares, A.C., Ferreira, A., Mariën, J., Delay, C., Lee, E., Trojanowski, J.Q., Moechars, D., Annaert, W., and De Muynck, L. (2021). PIKfyve activity is required for lysosomal trafficking of tau aggregates and tau seeding. J Biol Chem 100636.

Suzuki, K., Bose, P., Leong-Quong, R.Y., Fujita, D.J., and Riabowol, K. (2010). REAP: A two minute cell fractionation method. BMC Research Notes *3*, 294.

Vagnozzi, A.N., Li, J.-G., Chiu, J., Razmpour, R., Warfield, R., Ramirez, S.H., and Praticò, D. (2019). VPS35 regulates tau phosphorylation and neuropathology in tauopathy. Molecular Psychiatry.

Verstraelen, P., Van Dyck, M., Verschuuren, M., Kashikar, N.D., Nuydens, R., Timmermans, J.-P., and De Vos, W.H. (2018). Image-Based Profiling of Synaptic Connectivity in Primary Neuronal Cell Culture. Front. Neurosci. *12*.

Wen, L., Tang, F.-L., Hong, Y., Luo, S.-W., Wang, C.-L., He, W., Shen, C., Jung, J.-U., Xiong, F., Lee, D., et al. (2011). VPS35 haploinsufficiency increases Alzheimer's disease neuropathology. J Cell Biol *195*, 765–779.

Williams, E.T., Chen, X., and Moore, D.J. (2017). VPS35, the Retromer Complex and Parkinson's Disease. J Parkinsons Dis *7*, 219–233.

Woerman, A.L., Aoyagi, A., Patel, S., Kazmi, S.A., Lobach, I., Grinberg, L.T., McKee, A.C., Seeley, W.W., Olson, S.H., and Prusiner, S.B. (2016). Tau prions from Alzheimer's disease and chronic traumatic encephalopathy patients propagate in cultured cells. PNAS *113*, E8187–E8196.

Wu, J.W., Herman, M., Liu, L., Simoes, S., Acker, C.M., Figueroa, H., Steinberg, J.I., Margittai, M., Kayed, R., Zurzolo, C., et al. (2012). Small Misfolded Tau Species Are Internalized via Bulk Endocytosis and Anterogradely and Retrogradely Transported in Neurons *.

Wu, J.W., Herman, M., Liu, L., Simoes, S., Acker, C.M., Figueroa, H., Steinberg, J.I., Margittai, M., Kayed, R., Zurzolo, C., et al. (2013). Small misfolded Tau species are internalized via bulk endocytosis and anterogradely and retrogradely transported in neurons. J Biol Chem *288*, 1856–1870.

Wu, J.W., Hussaini, S.A., Bastille, I.M., Rodriguez, G.A., Mrejeru, A., Rilett, K., Sanders, D.W., Cook, C., Fu, H., Boonen, R.A.C.M., et al. (2016). Neuronal activity enhances tau propagation and tau pathology in vivo. Nat. Neurosci. *19*, 1085–1092.

Yoshimori, T., Yamamoto, A., Moriyama, Y., Futai, M., and Tashiro, Y. (1991). Bafilomycin A1, a specific inhibitor of vacuolar-type H(+)-ATPase, inhibits acidification and protein

degradation in lysosomes of cultured cells. Journal of Biological Chemistry *266*, 17707–17712.

Zang, R., Case, J.B., Yutuc, E., Ma, X., Shen, S., Castro, M.F.G., Liu, Z., Zeng, Q., Zhao, H., Son, J., et al. (2020). Cholesterol 25-hydroxylase suppresses SARS-CoV-2 replication by blocking membrane fusion. PNAS *117*, 32105–32113.

Zhao, N., Liu, C.-C., Van Ingelgom, A.J., Linares, C., Kurti, A., Knight, J.A., Heckman, M.G., Diehl, N.N., Shinohara, M., Martens, Y.A., et al. (2018). APOE ε2 is associated with increased tau pathology in primary tauopathy. Nat Commun *9*, 4388.